CFD study and manufacturing of a wing with winglets

For the improvement of a laboratory practice for
Aerodynamics

Javier Ferrero Micó

A thesis presented for the degree of
Aerospace Engineering - Aircraft Design

Tutor: Xandra Marcelle Margot

Escuela Técnica Superior de Ingeniería del Diseño
Centro de Motores Térmicos
Universitat Politècnica de València
Spain
Academic course 2016-2017

Abstract

This document shall detail all the processes followed for designing, calculating, analyzing and building four different wing geometries. The report starts with the theoretical introduction to the winglets' characteristics. Then, it shall explain all the steps followed in order to design the CAD models and how to tackle all the stages of the CFD analysis (preprocessing and processing). It will also include a section referring to the 3D printing process.

Once these preliminary phases are over, the document shall proceed to work on the postprocessing stage of the CFD calculus, in order to study the results obtained and compare the different geometries.

In the end conclusions will be reached about which geometry seems to be the best regarding the flight conditions established and further steps shall be presented in case this study shall be continued as another TFG or TFM.

KEY WORDS: winglet, CAD (Computer-Aided Desing), CFD (Computational Fluid Dynamics), 3D Printing, different geometries.

Resumen

Este documento detalla todos los procesos seguidos para diseñar, calcular, analizar y construir cuatro geometrías alares diferentes. Este informe empieza con una introducción teórica sobre las características de los winglets. Seguidamente, explicará todos los pasos seguidos para diseñar los modelos CAD y cómo abordar el análisis CFD (pre procesado y procesado). También incluirá una sección relacionada con el proceso de las impresiones 3D.

Una vez esta fase preliminar haya sido analizada, el documento procede a explicar el post proceso del cálculo CFD para estudiar los resultados obtenidos y comparar así las diferentes geometrías.

Finalmente, se concluye qué geometría presenta mayores beneficios en relación a las condiciones de vuelo establecidas y se plantearán posibles planes para seguir desarrollando el tema en otro TFG o TFM.

Palabras clave: winglet, CAD (Computer-Aided Desing), CFD (Computational Fluid Dynamics), impresión 3D, geometrías diferentes

Resum

Aquest document detalla tots els processos seguits per a dissenyar, calcular, analitzar i construir quatre geometries alars diferents. Aquest informe comença amb una introducció teòrica sobre les característiques dels winglets. Seguidament, explicarà tots els passos a seguir per a dissenyar els models CAD i com abordar l'anàlisi CFD (preprocessament i processament). També inclourà una secció relacionada amb les impressions 3D.

Conclosa aquesta fase preliminar, el document procedeix a explicar el post processament del càlcul CFD per a estudiar els resultats obtinguts i comparar les diferents geometries.

Finalment, es conclou quina geometria presenta majors beneficis en relació a les condiciones de vol establertes i es plantejaran possibles plans per a seguir desenvolupant el tema amb altre TFG o TFM.

Paraules clau: winglet, CAD (Computer-Aided Desing), CFD (Computational Fluid Dynamics), impressió 3D, geometries diferents

Declaration

I declare that this thesis has been composed solely by myself and that it has not been submitted, in whole or in part, in any previous application for a degree. Except where states otherwise by reference or acknowledgment, the work presented is entirely my own.

Acknowledgements

Contents

List of Figures

List of Tables

"There is no sport equal to that which aviators enjoy while being carried through the air on great white wings."

Wilbur Wright, 1905

1

Introduction

Since the beginning of the aviation history back in the Wright's workshop until now, the aerospace industry has achieved to be one of the technological leading fields in innovation and cutting-edge scientific research. The aerospace sector has empowered the Globalization and nowadays it is fighting for increasing the efficiency and improving the performance of its products and prototypes.

Amongst all the outcomes provided by the sector, we shall focus on aircrafts and their aerodynamic behavior. For them to fly, airplanes count with lifting devices that provide them with the necessary upwards force to beat the gravity force and take off. Aside from the Lift force, the Drag force is also generated. This is the aerodynamic resistance that affects the flight of an airplane. There are several types of resistance, but this project shall be centered on the drag induced by the lift generation.

The first question is, how is lift generated? This aerodynamic force appears when there is a difference of pressure between the intrados (high-pressure) and the extrados (low-pressure). The imbalance of this pressure distribution shall generate lift. As for a 2D case, we can see in Figure 1.1 the resultant forces generated.

Nonetheless, as ours is a 3D case, there is a span wise direction flow vector which moves towards the root on the extrados and towards the wingtip in the intrados. This 3D component will affect the overall aerodynamic properties as presented in Figure 1.1.
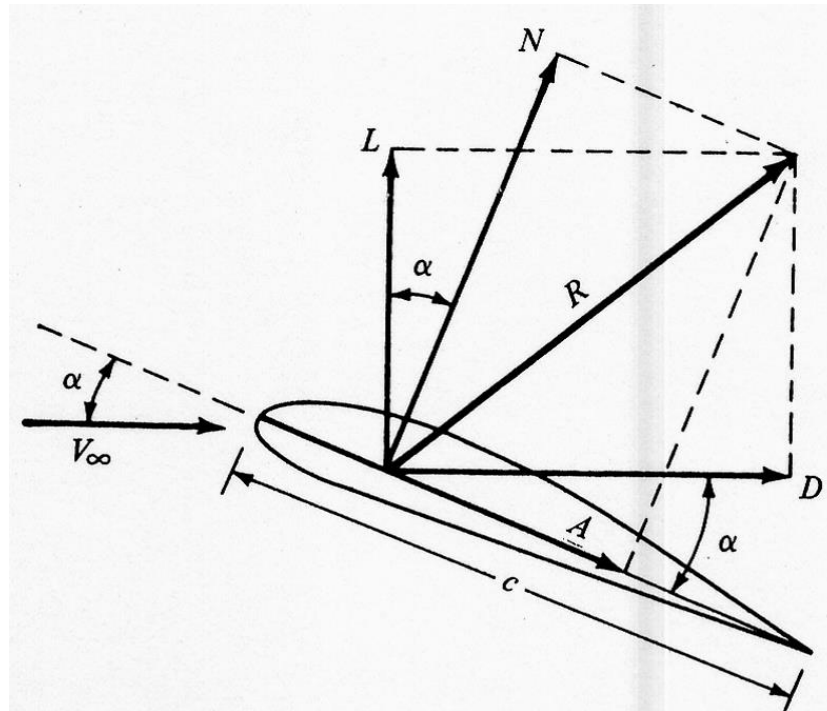
Figure 1.1: Resultant aerodynamic force and the components into which it splits [12]

In Figure 1.2. is it possible to see the cause of this wingspan vectorial component. The flow is forced from the high-pressure intrados to the low-pressure extrados making it to curl around the wingtips [12]. This motion is known as circulation and it is the result of lift generation. In Figure 1.2 it is also possible we can identify the existence of a vertical symmetry plane which will help to our design task, as it will only be necessary to study half of the airplane's geometry. [see 26, Online article]
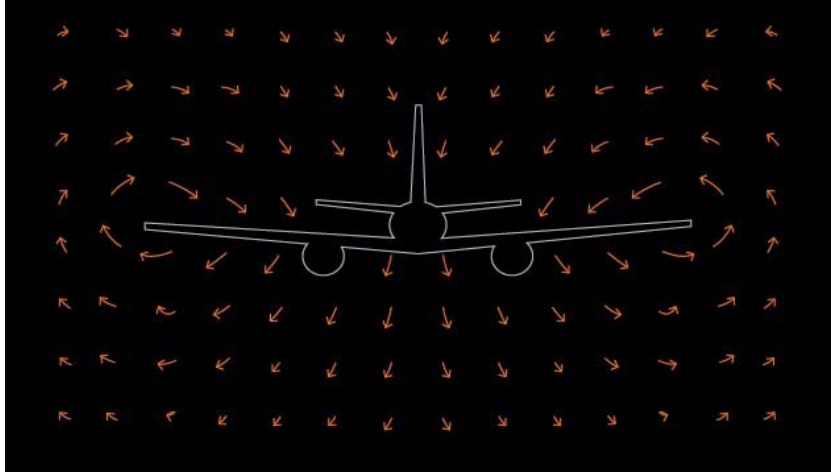
Figure 1.2: Motion of the air behing a lifting wing without winglet [26]

This circulatory motion of the flow generates trailing vortexes at each wing tip. In Figure 1.3, we can see how these vortexes look like. The arrows represent the streamlines deviations due to this 3D flow component, which at the wintips results on this "tornadoes"-like flow movement.

The vortexes spotted on Figure 1.3. shall induce a downwards velocity component to the airflow, which is called down wash, noted by w in Figure 1.4.
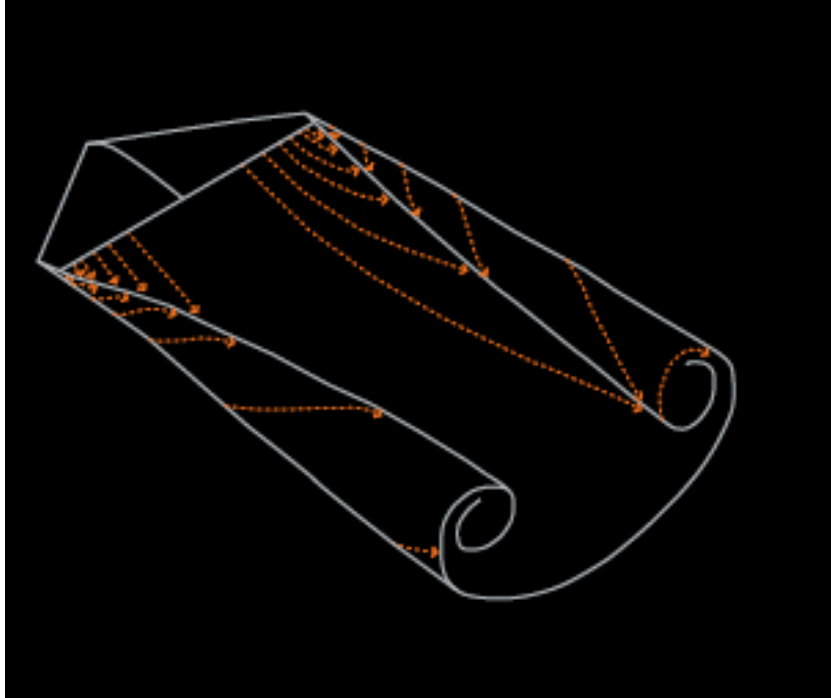
Figure 1.3: Vortex wake behind a lifting wing [26]

In order to understand the following explanation, we shall bear in mind that we have a geometric angle of attack, α, and the induced angle off attack α_i which is generated by the downwash velocity component. It will therefore incline the local relative wind as shown in the Figure 1.4. This effect shall have two main results [see 12, chapter 5]:

- On one hand, the effective angle of attack α_{eft} shall be obtained as shown in Figure 1.4, which will be therefore locally smaller than the geometric one.

- The Local lift vector is also tilted by the α_i angle as shown in Figure 1.4. Therefore, the Lift is decomposed into two new vectors, one of which appear in the direction of the free-stream velocity which is the same as the Drag overall direction. Thus, downwash induces a drag force, noted as D_i which stand for Induced Drag. In order to isolate the Induced Drag, the angle of attack will be set to 0.
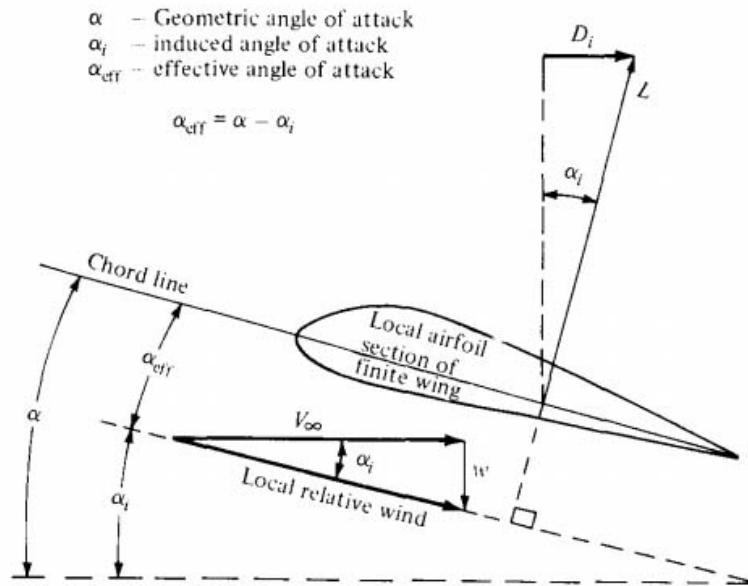
Figure 1.4: Induced drag generation [12].

Intuitively we can recognize from the previous schemes that there are several factors which influence the Induced Drag; wing span (either horizontally or vertically) is the main feature that will affect the size of the vortexes generated and their relative position with respect to the wing (which will affect their influence towards the pressure distribution on the lifting surfaces). Another important factor will be the induced angle of attack, which is product of the downwash velocity vector, directly linked to the intensity of the vortexes and therefore linked to both Lift and Drag generation. Amongst other strategies, this improvements can be achieved by implementing wingtip devices such as winglets in order to control the local curl of the flow.

Winglets allow to reduce the wing tip vortexes size and they prevent their interference with the wing boundary layer as they are generated far from the wing lifting surface. They also increase their spreading along the wing Trailing Edge, fostering the lift generation at the wingtips. They should be carefully designed in order to minimize their weight in order to avoid structural problems such as bending momentums at the wing root. Depending on their configuration they can also contribute actively to the lift generation (in the case they are not normal to the wing). Other features can be inplemented

such as a sweep angle as in the Raked configuration which improves cruise performance or toe-in angle which reduces the aforementioned bending momentum generated by the weight at the wing root.[see 14, p35]

In order to gather consistent information for conducting a conclusive project, it will be necessary to solve the Navier-Stokes equations for each of the geometries implemented. This will be done by a Computational Fluid Dynamics calculations, which consists on performing calculations via numerical analysis in order to simulate the interaction of the fluid with the geometries, which are defined by the boundary conditions.

As a result, it will be possible to understand how the flow behaves around our wings geometry thanks to both numerical and graphical data given by the CFD resolution of our problem.

2
Objectives

The problem we are going to face, as stated previously, will be related to winglets and how different configurations affect, if so, the general performance of the aircraft.

This document shall analyze four main configurations. Three of them are geometries that can be seen on the most common flying airplanes. In order to try to isolate their effect, they will all be installed on the CAD wingtip of the same wing. The A320 wing geometry has been chosen for this purpose.

The fourth one will present no winglet ending. This geometry will be build by performing a cut where the winglet should be placed. This case will be used to check the differences among the geometries if any, and try to decide which of them is better.

It will also be possible to analyze the effect of the sweep angle, which in one of them will evolve along the horizontal plane, whereas in other two of them will be a constant vertical angle, applied on their wiglet's leading edge (LE).

The designs developed shall be implemented in the Ansys 18.0 Software,

provided by the University. They will also be printed in 3D in order to provide models for the wind tunnel Lab Practice. The 3D printed prototypes do represent the validation stage that any industrial innovative procedure needs to fulfill.

By following these steps, this project shall achieve:

- To update and improve the Lab Practice performed in the Aerodynamics course by providing students with a brand new problem to solve. Thanks to the 3D solid models and the software models, they will be able to contrast the work procedures when using numerical methods vs experimental data.

- To analyze the flow behavior on each of the geometries and decide if there is any configuration among those studied with better qualities than the others. It will allow to check in which cases a winglet has a good performance.

- To encourage further investigations on the topic from an academic point of view, so that students can learn more about these complex cases. The knowledge gained will be useful for them in their future careers as engineers. This preliminary study can be the starting point for other TFG or TFM where new geometries can be developed.

This project will allow to gain knowledge on the design and manufacturing processes for aeronautics model prototypes, it will help to understand how CFD calculations work and how do they need to be Set Up in order to perform a proper analysis. It will also explain how to approach the post processing tasks, how to gather results and how to present them.

All in all, thanks to this project it will be possible to see how industry works when they need to generate a new design by always checking previous models in order to have a starting point (as we could learn in Aircraft Calculus subject) and performing preliminary numerical analysis on the desired geometries. This project will also provide the tools for validating the software results by using a wind tunnel.

3

CAD Design

3.1   Winglet Geometries

The first step in order to analyze and manufacture the geometries is to design them on a CAD developer. The four configurations' digital design will be the foundation on which it will be possible to settle the wall boundary conditions on the ANSYS CFD solver afterwards.

The reader must bear in mind, as already stated in the introduction section, that all the configurations chosen exist and they are currently used in most aircrafts. In fact, in the following Figure, it is possible to look at examples of real aircrafts with diverse winglet types:

These are the four configurations:

(a) No winglet configuration

(b) Blended winglet configuration

Figure 3.1: Different winglet configurations: Part I.

(c) Raked winglet configuration

(d) Endplate winglet configuration

Figure 3.1: Different winglet configurations: Part II.

The image a) shows a wingtip without any refinement. A cut, parallel to the airfoils' plane, has been performed. This configuration can be seen on small aircrafts that fly at low speeds. This configuration is being implemented within our study in order to see the flow usual behavior, i.e. how the intrados interacts with the extrados and how this affects the lift generated.

In image b), Blended configuration is presented. The first Blended winglets were installed on Gulfstream II airplanes. While this is one of the main configurations for Aviation Partners Inc. airplanes (Falcon Series, Hawkers series and Boeing Business Jets series) and they have put a lot of effort on it as we can see on the quote next to this text which is from the Aviation Partners Inc. Corporate Website, Airbus tested two prototypes and finally determined that their benefits were not so interesting. They did not develop them further. These facts already show that there is not a common ground on which are the best winglets and that is why this project's topic is so interesting.

> "Blended Winglets are the single most significant aerodynamic improvement ever developed for commercial or business aviation."
>
> Clay Lacy, Aviation Partners Inc. Founder and CEO [see 9, Homepage]

This kind of winglet behaves as upwards extensions of the airplane wings. They include a sweep angle which is combined with a smooth chord variation in the transition zone. According to some research performed by Boeing, this should help in reducing some of the viscous drag while sacrificing a part of the potential induced drag reduction. [26]

Image c) shows a Raked design implemented by Boeing. In Raked wingtips the designer has to add extra wingspan in order to fully develop the geometry of this winglet. This can sometimes affect the aircraft's performance, limiting the airports where they can fly in case there are some gate limitations for certain wingspan values. Another feature is that the leading edge at the tip will have a much greater sweep angle than the leading edge of the main wing. [18]

Raked winglets have proven to be efficient for really long range flights as they optimize the cruise phase by reducing the fuel consumption.[1]

Finally, the fourth configuration is shown in image d). The Endplate configuration is pretty common among some of the A320 series. It is the oldest design and for over a century, it was the most used device. Nevertheless, for it to be 100% effective, there are some theories that support the fact that the winglet should be so large that its surface would generate more skin friction than the induced drag reduction it could imply. [15] In the following sections we shall check whether this is totally true or not.

The next step is to implement the designs presented in CAD. The wing measures and shape have been taken from the AIRBUS A320's Airplane characteristics for Airport Planning manual. [see 22, Chapter 2-Section 220]. Thanks to the schemes that can be found in this manual, the dimensioning of the airplane features has a realistic approach. On the same manual, the flight conditions can be found. Those will be applied and explained later on, in the Set Up section [see 22, Airplane Performance Section].
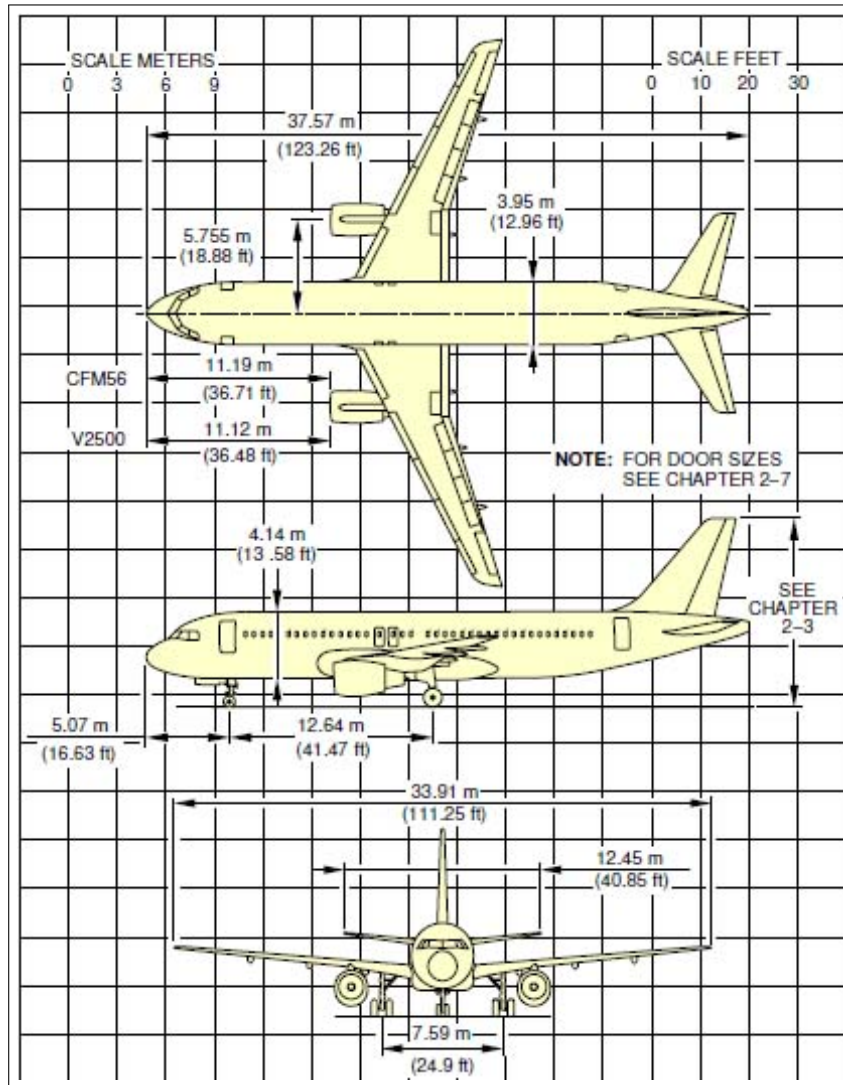
Figure 3.2: A320-100 General Airplane Dimensions [22]

3.2   Wing Airfoil

Following with the idea of approximating the model to a real aircraft and taking into account that it has been impossible to learn which airfoil AIR-BUS uses in the A320 SERIES, it was decided to choose an airfoil based on the criteria explained below.

Aside from the induced drag, when flying at high speeds, near to transonic regime, shock-waves can appear and if they do so, they will generate drag. In the early 1970s, studies where performed by NASA at the Dryden Flight Research Center in order to develop what we nowadays know as super critical airfoils (SPA). These airfoils allowed to design super critical wings (SPW) which are now used on business jets, airliners and transports, and numerous military aircraft (such as the F-8 fighter)[24] as they are more efficient in near-sonic flight conditions and they reduce the fuel consumption.

Whereas conventional NACA airfoils are rounded on the top part and they are nearly flat on the bottom part, the supercritical airfoil are flatter on the extrados and they present a more or less sharp bend on the intrados. On the lower part of the trailing edge this curvature is stressed with a upwards arc whose aim is to restore the lift gone due to the flat upper surface. See Figure 3.3 in order to see a scheme of both airfoils and their performance in cruise conditions.
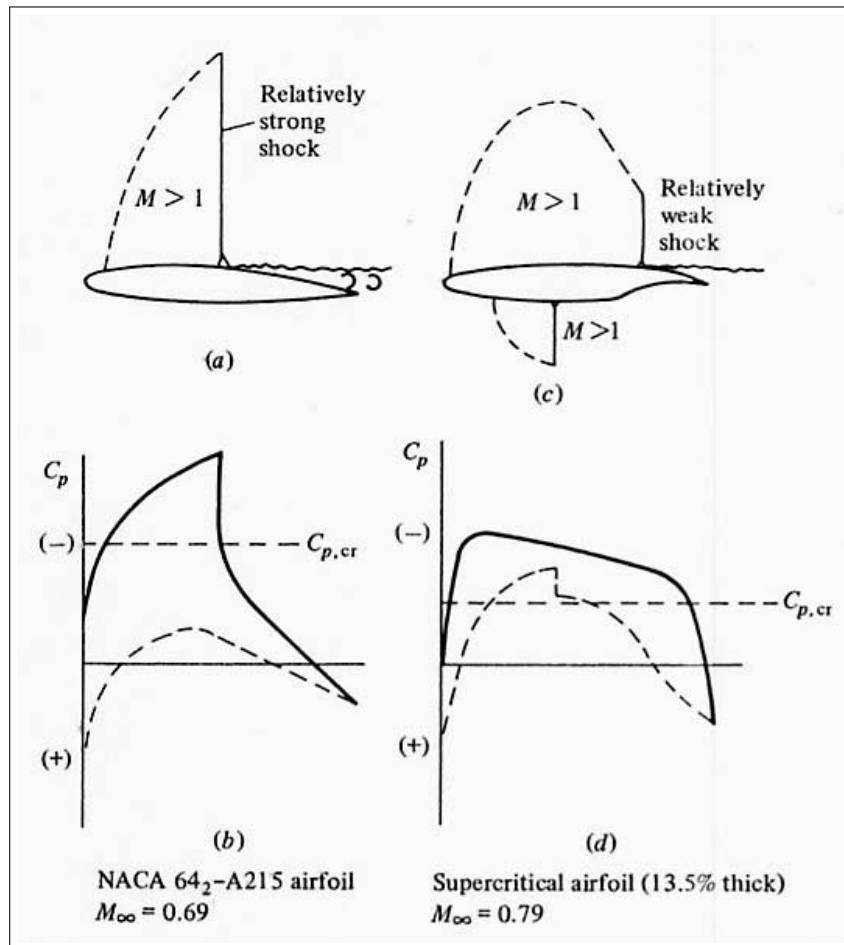
Figure 3.3: NACA 64 series airfoil vs supercritical airfoil at cruise lift conditions [14]

As we can see in Figure 3.3, when flight conditions match speeds near Mach 1 (sound speed), as the curvature at the extrados accelerates the airflow, it can become supersonic. This increasing speed can generate a sudden pressure gradient which appears as a shock-wave.

In the case of the NACA airfoil, as we can see in Figure 3.3, these flight conditions can deteriorate the overall performance of the airplane as a relatively strong shock-wave can appear in an zone relatively near to the LE which may induce a separation of the airflow boundary layer and generate

turbulence. The separated wake will increase drag, fuel consumption and it can cause structural issues such as buffeting or a drop in velocity which at the extreme can cause stall conditions.

As it can be observed in Figure 3.3, although the Mach number of the free-stream flow is higher in the supercritical airfoil case, the shock wave appears closer to the trailing edge as it is delayed to higher Mach numbers. Its strength will also be diminished. That will mean a reduction on the drag generated as the boundary layer detachment, in case it appears, will do so later than in the NACA airfoil. This happens due to the flat extrados which causes less acceleration on the flow. As a drawback, this flat extrados will mean a reduced production of lift. In order to compensate this loss, the increased curvature on the intrados close to the TE is meant to improve the lift generation.

Thanks to this technology, aircraft flight conditions can be set for higher subsonic cruise velocities. From a financial point of view, it also means that airliners and business jets can reach farther destinations in less time and with less fuel.

As will be seen in the following sections the prototype flight conditions will be set to Mach=0.76. This means that at cruise conditions we would potentially get supersonic conditions at some parts of the airfoil if the airfoil would be a conventional NACA airfoil. In that case, the shock waves that could appear might interfere with the effect of the winglets on the drag and lift generation. Thus, in order to get clear results, and avoid as much inter-ference as possible, we shall choose a supercritical airfoil as the most suitable option for this project [17].

Once settled the idea of choosing a supercritical airfoil, which one should be chosen? As the study is about commercial aircrafts, and since it is known that wings serve as fuel reservoirs in these, it seems about right to choose a thick airfoil.

After all these facts have been exposed, the chosen airfoil corresponds to one of the geometries that were used as an experimental model during the de-velopment of supercritical airfoils by NASA in the Langley Low-Turbulence Pressure Tunnel: the **SC(2)-0714** See Figure 3.4.
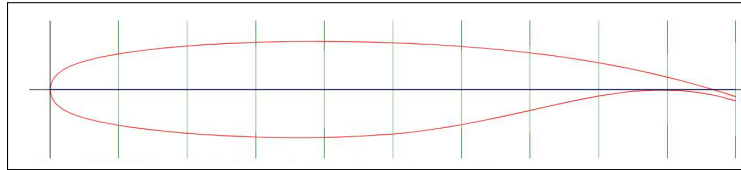
Figure 3.4: SC(2)-0714 Supercritical airfoil (Ref. NASA TP-2890)

Figure 3.4 has been plotted by the on-line platform $airfoiltools.com$ which is an on-line database for searching, comparing and plotting airfoils. The list of coordinates that allow us to plot the airfoil presented in Figure 3.4, can be also found on the in the NASA Technical Paper 2969 [see 10, p36]. In the Figure 3.5, we can also see the plots provided by the same $airfoiltools.com$ platform for the lift and drag coefficients for different Reynolds numbers vs angle of attack.

(a) CL vs angle of attack

(b) CD vs angle of attack
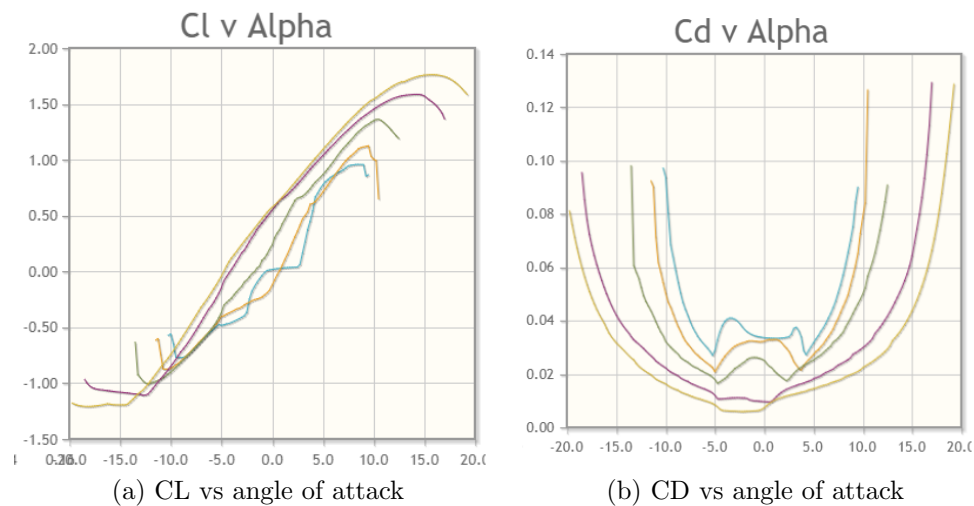
Figure 3.5: Aerodynamic curves for SC(2)-0714.

Reynolds Numbers: Blue = 50.000; Orange = 100.000; Green = 200.000; Pink = 500.000; Yellow = 1.000.000

For further details about this airfoil, check the NASA Technical Paper 2969 [see 10, p15] and the Paper Aerodynamic Performance and pressure distributions for NASA SC(2)-0714 Airfoil tested in the Langley 0.3-Meter Transonic Cryogenic Tunnel [19]

3.3   Winglet Airfoil

With regard to the winglet airfoil, each of the four configurations presents a different approach. For the no-winglet configuration, the same SC(2)-0714 has been used as a limiting plane to close the geometry. The other three wingtips are based on of the symmetrical airfoil we can see on Figure 3.5. It has been chosen because winglets are built out of thin airfoils. We also would like to avoid any lift or drag generation due to the winglet geometry, and this is why the airfoil should be symmetric. In this way, if the winglet generates any lift or induced drag it will be due to the 3D-flow effect and not to its configuration.
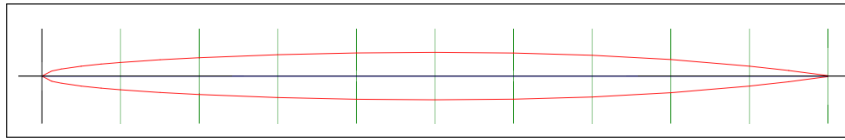
Figure 3.6: NACA 16-006 airfoil

As in the previous case, we can see in Figure 3.6 the plot for the airfoil chosen which is the NACA 16-006. This graph, as well as the ones that can be seen in Figure 3.7. have been provided by *airfoiltools.com*. Figure 3.7. shows the lift and drag coefficients for different Reynolds numbers vs angle of attack.

(a) CL vs angle of attack   (b) CD vs angle of attack
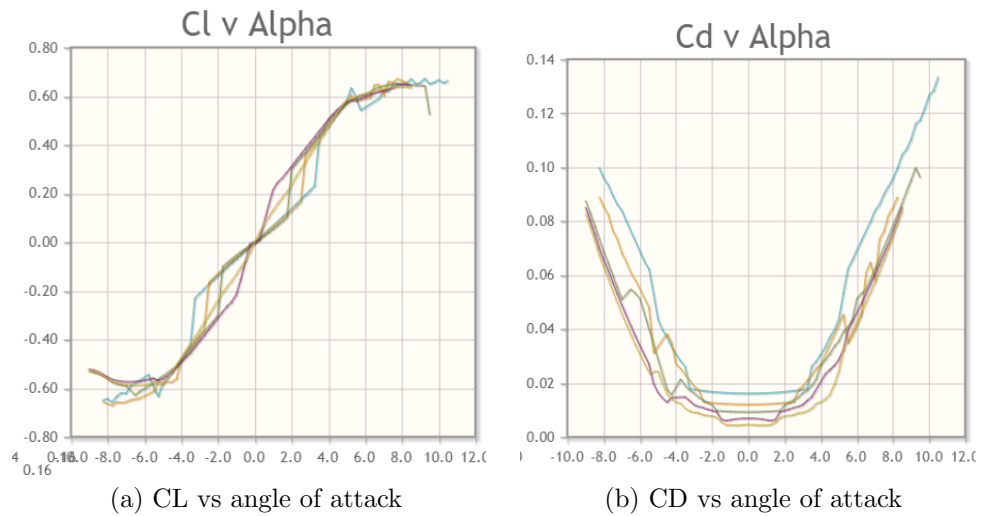
Figure 3.7: Aerodynamic curves NACA 16-006 AIRFOIL.

Reynolds Numbers: Blue = 50.000; Orange = 100.000; Green = 200.000; Pink = 500.000; Yellow = 1.000.000

3.4   3D Design

Once the airfoils are chosen and the general shape has been decided based on the A320 sketches, it is time to merge all this information and generate the CAD models. In order to be sure that we can analyze the winglets as isolated as possible, all the models have been given the same fuselage.

Additionally, for us to be able to use the same design for the CFD analysis and the manufacturing process, in Figure 3.8 we can see how the fuselage designed is empty inside for reducing the 3D Printing time. The yellow square on the Figure 3.8 a), shows the only section where the fuselage is completely solid. This part will host the bar which should hold the model on the wind tunnel's support:
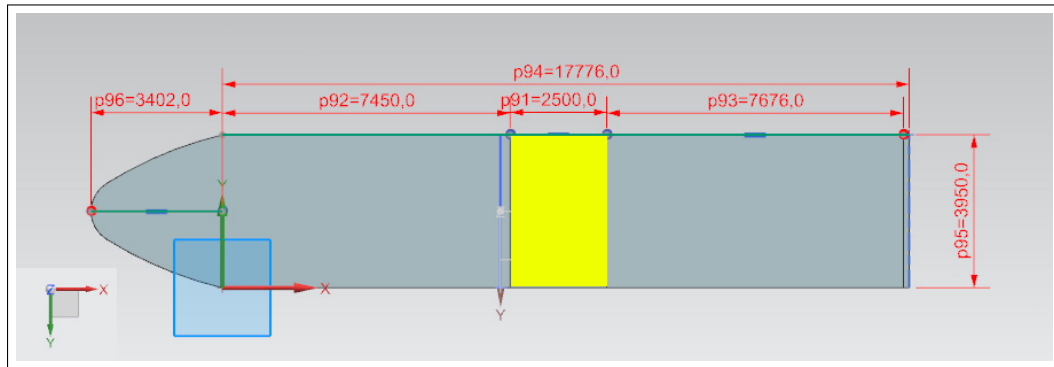
(a) Fuselage dimensions (mm)
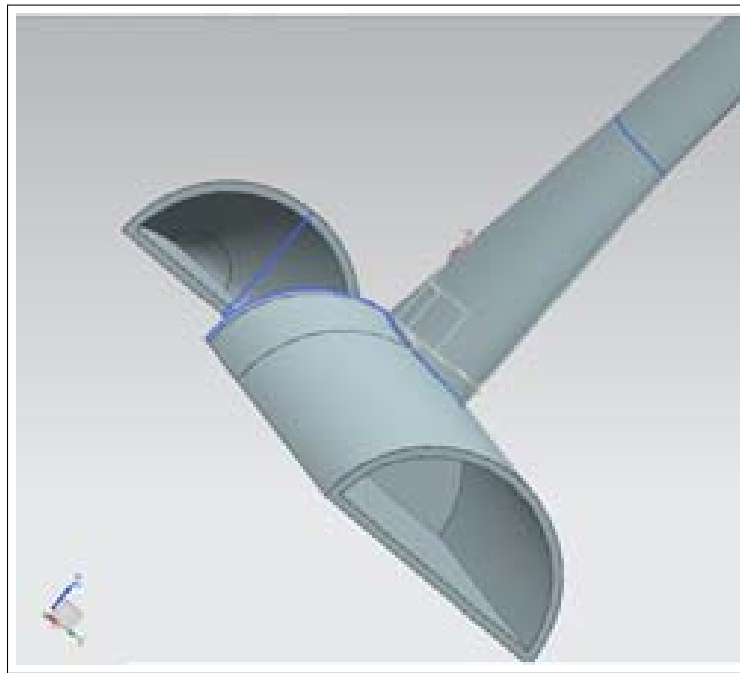
(b) Internal empty structure view and wing root

Figure 3.8: Fuselage dimensions and configuration

After being the fuselage designed, the basic wing structure is developed. It cab be seen in Figure 3.9 and it will also be the structure used for the **no-winglet** case. The other geometries will be added at the wingtip. In this way, we shall keep the horizontal standard dimensions for all the models as equal, and the addition of a winglet shall modify every aspect of the wing, as it was explained in section 3.1.
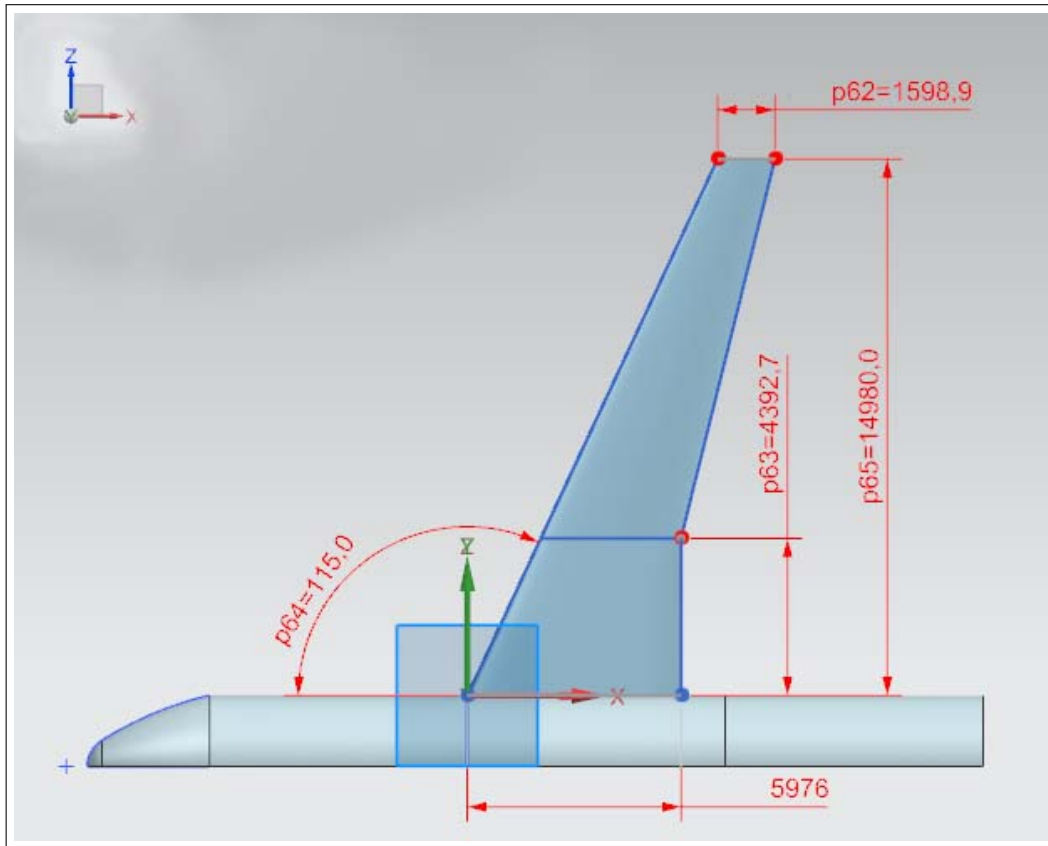
Figure 3.9: 3D CAD model - wing dimensions for no-winglet case (mm)

Then, in the following images, the dimensions for the other three wingtip devises are presented:
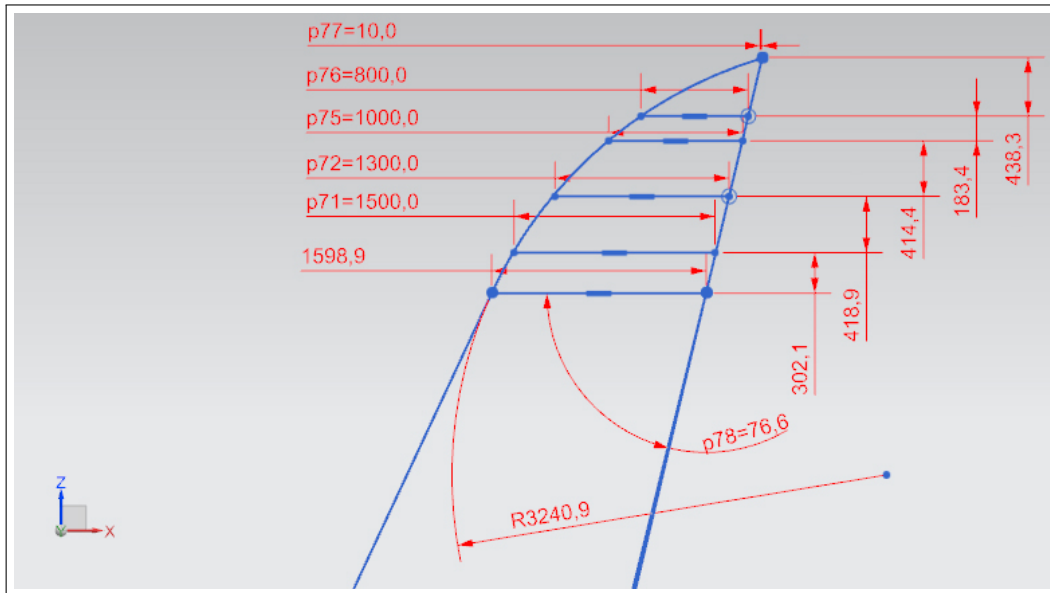
Figure 3.10: Dimensions for the raked winglet (mm), (º)

As we can see in Figure 3.10, the Raked winglet presents a progressive change in the sweep angle of the leading edge of the wing. The horizontal lines have been drawn in order to both guide the LE shape and help to the transition from the supercritical airfoil to the symmetric one.

As for the Blended winglet that we can see on Figure 3.11, both LE and TE present an angle. In case several flight regimes would be studied, its effect could be examined.

Similarly, the Endplate's configuration also present a leading edge angle, which is greater than the one on the LE of the Blended configuration. This can be observed on Figure 3.12.
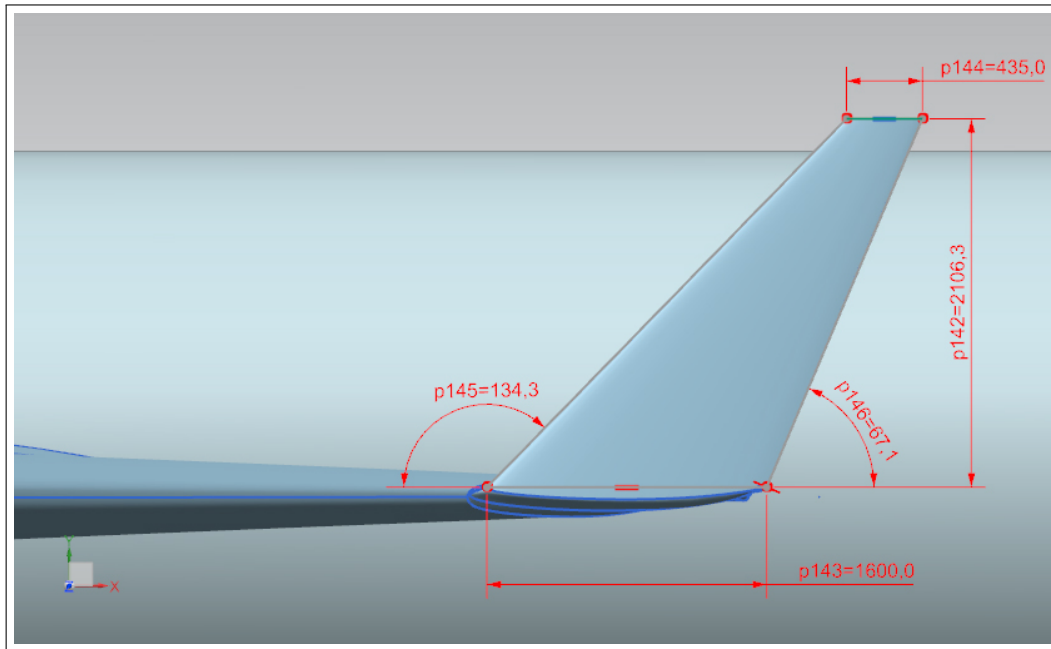
Figure 3.11: Dimensions for the blended winglet (mm), (º)
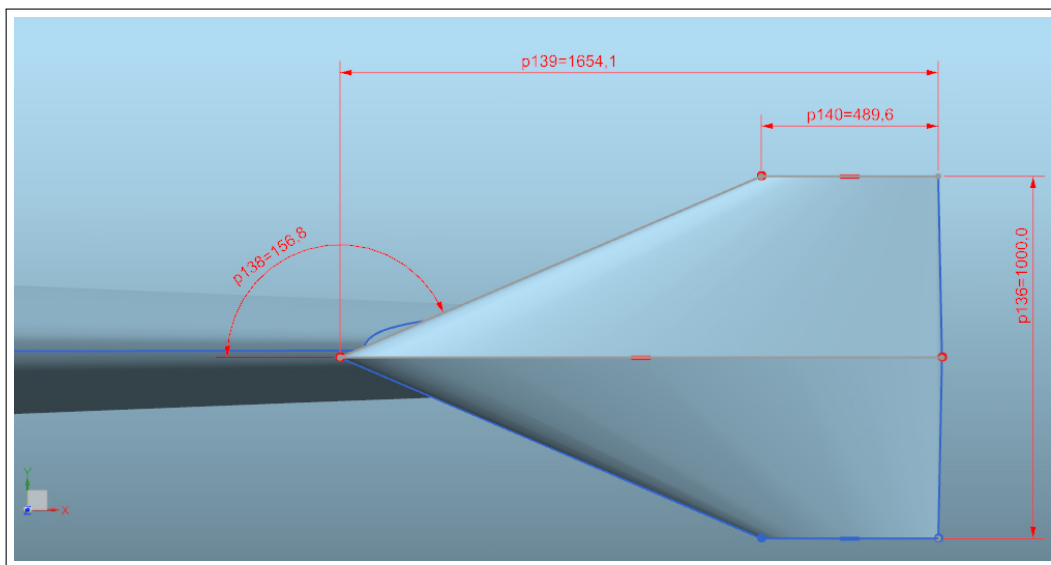
Figure 3.12: Dimensions for the endplate winglet (mm), (º)

Finally, as all the dimensions are clearly presented in Figures 3.9, 3.10, 3.11 and 3.12, all the geometries can be built. As it can be seen on these Figures, the measures highlighted show that these models have been built in 1:1 scale. This is so in order to be as exact as possible when following the schemes given by the A320 manual. In order to be efficient, as it will be explained later in the following section, the designs that will be used for the 3D Printing manufacturing process will have as foundation these ones. Therefore, they need to be escalated in order to fit inside the wind-tunnel. The scaling factor applied will be **1:50**.

In Figure 3.13., it is possible to see all four CAD Models with their symmetry plane and their reference system.

It can easily be detected that only one half of the model has been designed. As we presented at the introduction, the curling effect of the airflow is symmetric and FLUENT allows to generate a symmetry plane. Therefore our study will be performed as if it were analyzing a two-wings model although only half of it has been actually designed. This will reduce the designing time needed.
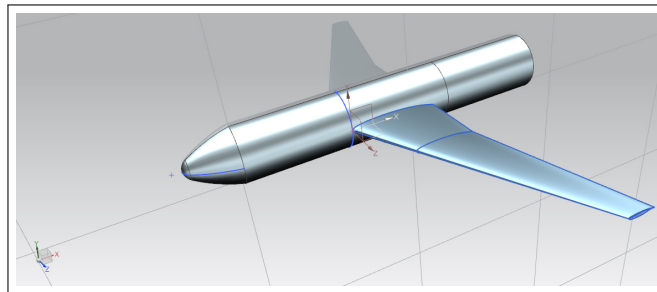
(a) No winglet configuration
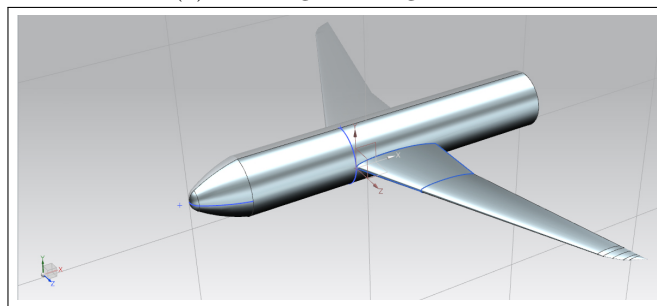
(b) Raked winglet configuration
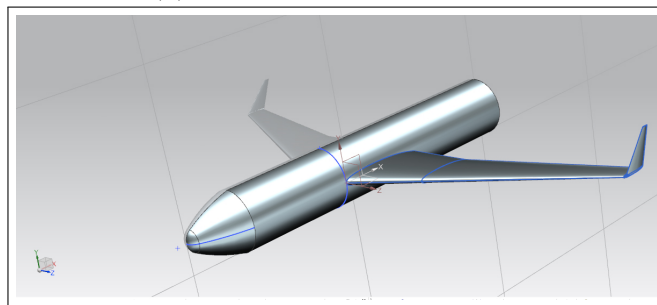
(c) Blended winglet configuration
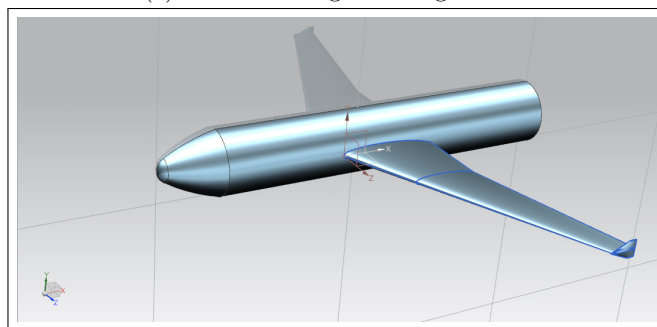
(d) Endplate winglet configuration

Figure 3.13: Different winglet configurations.

4

Manufacturing

4.1 3D Printing

Once the CAD designs are ready, it is already possible to manufacture the models for the wind-tunnel experiments. On this section the manufacturing process will be presented and explained. The reader will also be able to get to know a bit more about this technology.

Nowadays, many of the leading edge technological fields develop prototypes that need to be studied, tools and gigs specifically developed for concrete tasks or even fully functional devises that will not mean a big volume of production. 3D printing technology has enabled to build these models at lower costs as it is a fast method, which requires relatively small investments on the material used. This is an additive manufacturing process that generates a solid three-dimensional physical object out of any digital design desired by adding material layer after layer. It has applications in such different fields as medicine, architecture or as in our case, aerospace industry. [11]

At the ETSID, Zortrax M200 have been put on service for students to

develop their projects and these are the printing machines that have been used for the prototypes of this project.

The available workspace dimensions inside a Zortrax M200 are 200 x 200 x 180 mm. It is important not to stick to the maximum dimensions though, as it can imply a loss of quality when forcing the extruder and the system. On the grounds that these are fixed boundary conditions for the manufacturing process and taking into account that the model had to be bigger than those limits, the design had to be sliced.

Zortrax provides the Z-SUITE Software which allows a preprocessing of the model. Thanks to this tool, models could be accurately adapted. Therefore, the wing models which had been scaled with a scaling factor of **1:50**, had been cut, and now they present two new junctions, this is, three parts per each wing. We can see one example in Figure 4.1:

Figure 4.1: Manufactured Raked model

The material used is HIPS 800g pure black. This material has been chosen for its good surface finish and its strength. The black color has been chosen in order to ease the visualization of the streamlines that can be checked in the wind tunnel when fume is used to see how the flow behaves. As for the thickness of each layer, 0.14 mm is the selected value. In this way, the accuracy would be ensured and the time needed would be reduced.
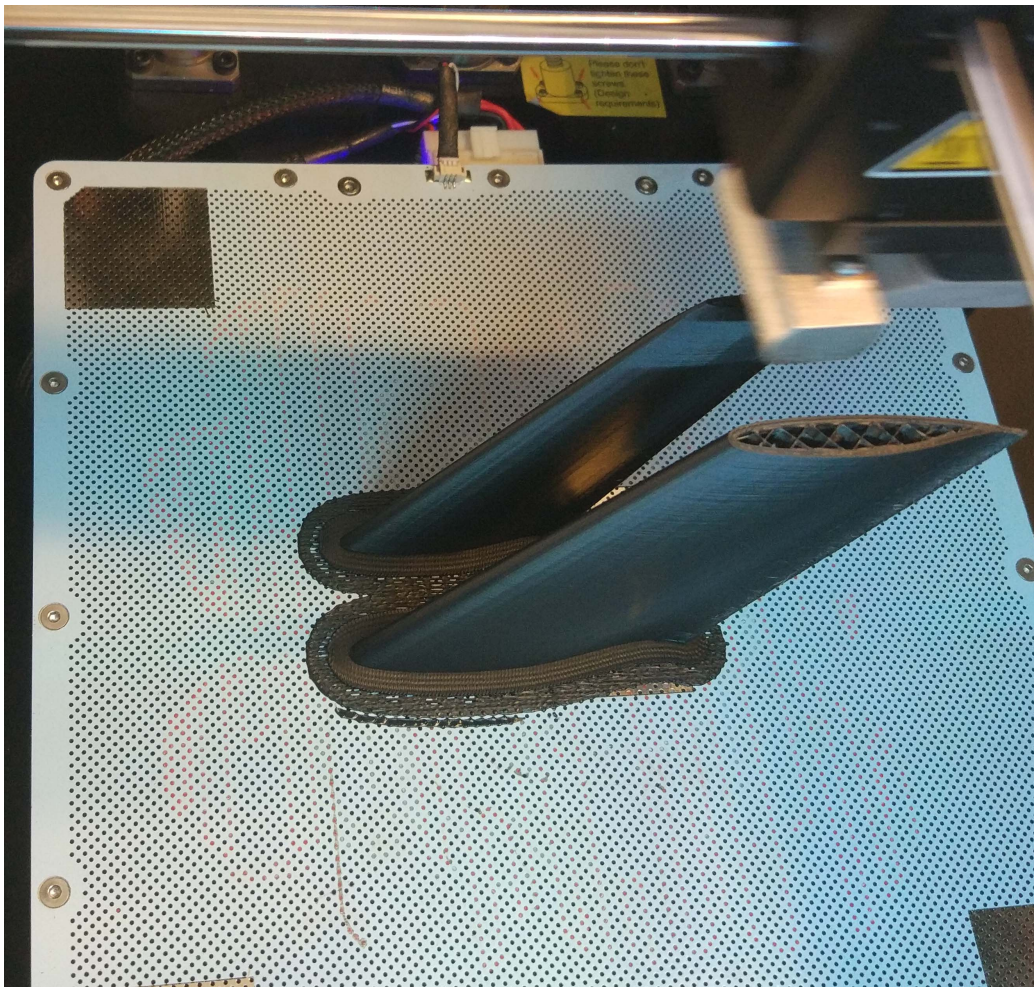
Figure 4.2: View of the printing procedure

The needed time for printing each of the pieces oscillated between 5h and 17h. This is why, aside from the thickness selection, other measures for time

reduction had to be implemented. As the models have been set to be solids, they are not empty in the inside. Filling the wing implies a big amount of time and material invested that can be reduced by setting it as low on the Z-SUITE software. This option ensures that an inner structure is generate which gives structural strength to the whole piece while reducing the manufacturing time needed and the material used. This filling can be seen on the Figure 4.2 above.

Another measure applied has been to cut the fuselage's front and rear part. These sections can be added later, as they can be manufactured by other means and there is no need for the 3D printing technology.

4.2   Assembly

Once all the pieces have been printed, it is time to assemble them as one whole solid. The outcome models, will have to stand the stress that the wind tunnel will put on them and they should keep their geometry and their properties. In order to achieve this, a hole shall be performed on each of the parts. Inside these holes an iron bar shall be placed.

As for the dimensions and location, each bar will be placed at on the thickest part of the airfoil. Then, these bars will have two sizes, the thickest ones will be of 2mm diameter and the thiner ones 1.5 mm of diameter. The thin bars shall be used for the top slices, where the thickness of the airfoil can compromise its integrity if a greater bar is assembled inside the holes.

One problem has been encountered when performing the holes, which is that the material melts due to the friction of the drill. This implies that it gets sticked on the blade and the hole looses accuracy if not treated carefully. Another important data is that the material can be melted with Universal Solvent for paint. This is a great asset as the material can be easily removed from the drill. Another issue encountered is related to the gaps inside the models due to the low filling option. Ones the hole is performed, the bar does not stay as still as it would be desirable. Therefore, extra glue will be needed in order to fix both the bars and the airfoil surfaces together.

In Figure 4.3 it is possible to see the final outcome for three of the models. The fourth one shows the supporting bars described:

Figure 4.3: No winglet, blended and endplate models built. Raked model showing the inner supporting structure.

5

Preprocessing

5.1   Design Modeler

All engineering simulations are based on a geometry which represents the design which wants to be analyzed. Within the ANSYS Workbench there are several tools that allow the integration of CAD models for their analysis. This integration is the first step of the preprocessing stage.

From all the options available, for this project the ANSYS Design Modeler application has been chosen. This tool has been designed in order to enable the edition of any existing CAD models. It is a parametric feature-based solid modeler which intuitively allows the drawing of 2-D sketches, the modeling of 3D pieces or to upload 3D CAD models from other CAD developers such as SolidWorks or NX Siemens.[see 2, Section:CAD Integration/Design Modeler User's Guide].

In order to proceed to the next step of the preprocessing, the CAD model needs to be inserted inside a fluid enclosure which will work as control volume for the subsequent calculations. Nevertheless, the first point that needs to be covered are the named selections on the CAD model. They are based on

bodies, surfaces or edges which were already defined by the CAD developer. These featured selections will allow later on to select values of the fluid on them. Therefore, the three main named selections established on the CAD model will be related to the surface on the extrados, the intrados and the winglet.

Once they are generated on all four geometries, the following step is to define the symmetry plane which will be transferred to the Mechanical application as a coordinate system. It will be related to the plane surface of the fuselage which is cut by the symmetry plane we designed before (It can be seen on the Figure 3.12.). To better see this feature, it is shown on Figure 5.1.:
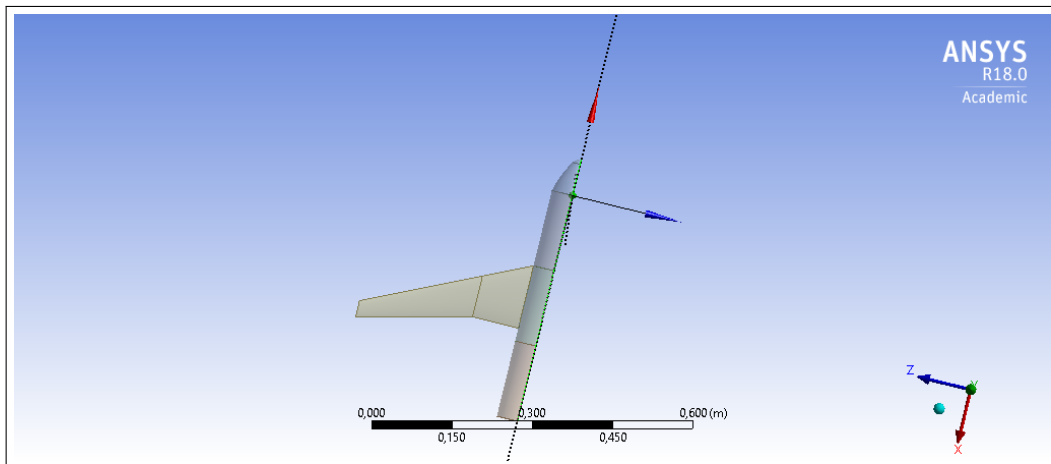
Figure 5.1: Symmetry plane

Then, based on this plane, after unifying all the bodies by means of a Boolean unite operation, it is time to set the enclosure that will work as control volume.

The enclosure feature is a tool used to encase the bodies of the model so that the material surrounding them can be set to a fluid whose physical and chemical characteristics shall be settled later on during the Set Up process.

This feature creates a frozen body around the selected bodies and then cuts them out from the enclosure. This operation does not erase the bodies

an therefore a new Boolean subtraction operation needs to be performed using as tool body the geometry from the CAD Model.

With regards to the dimensioning of the control volume, it has a box shape with a non-uniform cushion. The symmetry plane is integrated in it. As the partial model option is be selected, the program will understand it as a mirror and it will take into account the reflection of the model to the other side of the symmetry plane. Finally two more named selections shall be generated: symmetry for the symmetry plane and pressure-far-field for the other five surfaces of the enclosure. They will be useful later during the Set Up of the boundary conditions.

In the following two Figures 5.2 and 5.3, the reader will be able to see the general layout that the control volume will present and the dimensions of the box. This control volume shall be the same for all four geometries.
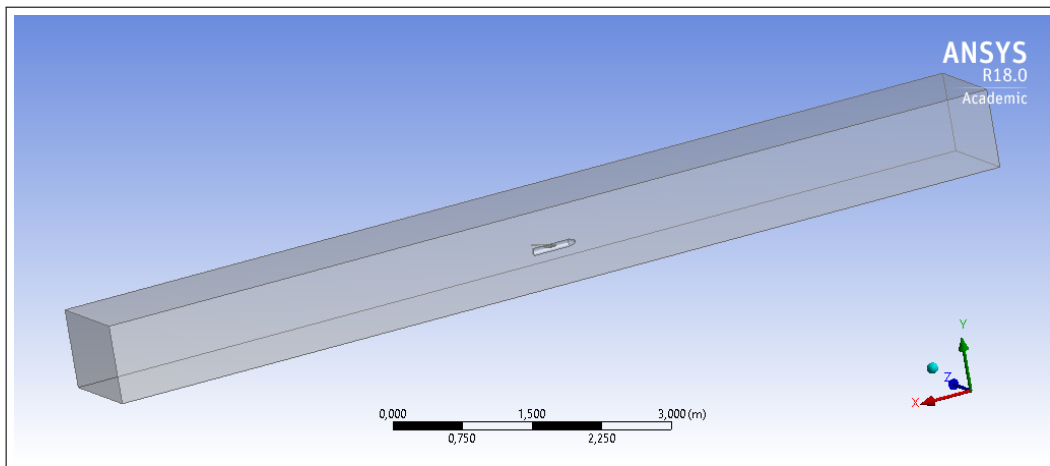
Figure 5.2: Symmetry plane
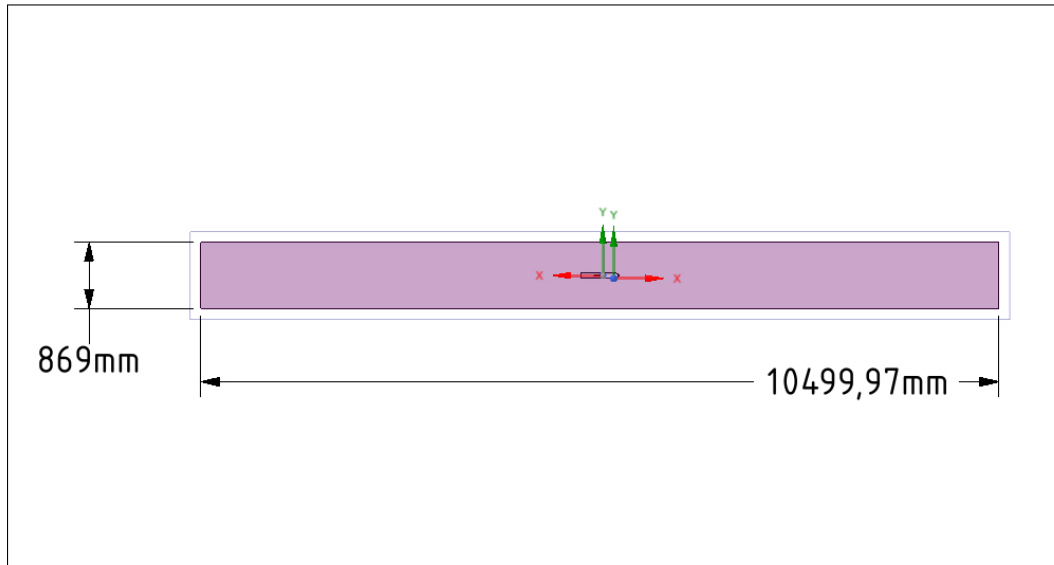
(a) Side view
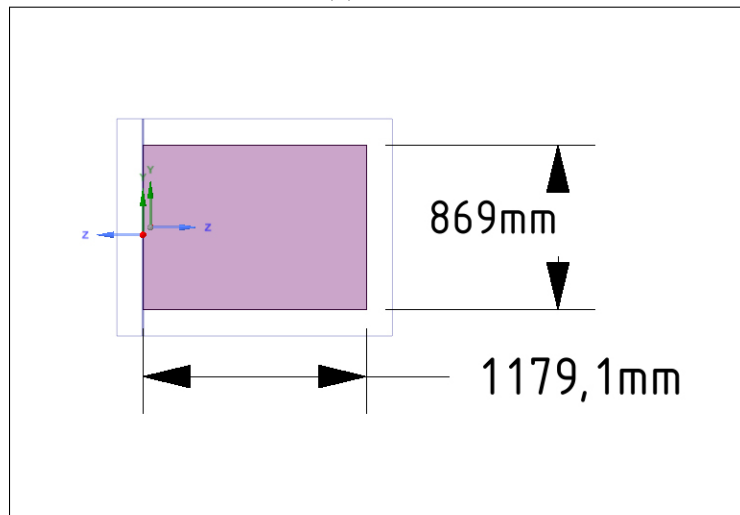
(b) Front view

Figure 5.3: Enclosure dimensions - ANSYS Spaceclaim

5.2   ANSYS Meshing

Fluid flow is governed by partial differential equations. As we shall work on steady-state conditions these will be the general Reynolds-averaged Navier–Stokes (RANS) equations for energy and turbulence model.

The Navier-Stokes equations describe the fluid flow behavior on a large number of problems by assuming it is a continuum with a high accuracy. Nonetheless, it is currently impossible to solve them for complex cases due incapability of representing the velocity scales and unsteady variations which are implicit in them.

One way to get consistent solutions is to decompose them into RANS, which enables the possibility to simulate practical engineering cases such as the flow over an aircraft. The assumption made is that the unsteady turbulent velocity fluctuations can be separated from the mean flow velocity. This method will then introduce a set of unknowns which require a turbulence model (they will be explained in the Set Up section) in order to produce closed systems of solvable equations.

As their computational requirements are reduced, it is possible to combine RANS equations with assumptions that enforce the conservation of energy and mass. This is the approach used in CFD which then breaks down the fluid domain into discrete cells by means of a mesh or a grid and then it solves the RANS and conservation laws in each of these subregions. The accuracy the results will have depends on the mesh element quality and orthogonality and on the turbulence model chosen [23].

It is also important to ensure proper continuity of the solutions across common interfaces between two subdomains, so that each of the subsolutions can be merged together with the others and then get a complete picture of the fluid flow in the entire domain.

There are several types of meshes that can be applied. On the one hand we have the structured mesh which is characterized by regular connectivity that can be expressed as a three dimensional array. This kind of mesh limits to hexahedra the geometry of our elements. On the other hand, the

unstructured mesh is characterized by irregular connectivity and cannot be expressed as a three dimensional array. It requires larger storing memory but it allows to use any geometry we might need. In our cases, tetrahedrons have been selected so our mesh shall be unstructured. [5]

Thanks to the named selections settled in the Design Modeler, the mesh can be accurately built by picking those surfaces and reducing the cells size or the growth rate. These modifications have been added to all the models on the extrados, intrados and winglets surfaces. In this way, a more precise mesh has been built around the geometries of interest leaving bigger cell sizes on the far field. This procedure has needed several iterations as when the calculation process was launched in Fluent, if the mesh were too big, the laptop would not be able to run it. This has been the case as the initial guesses where around 15.000.000 cells but it had to be reduced as the computational capacity of the computer was unable to handle these files. The current average amount of cells is 2.000.000 and the average number of nodes is above 500.000.

Besides the cell size, another option must be included. The mesh should perfectly adapt to the geometry and an outstanding resolution of the flow features must be ensured without this implying a big increase in the computational effort. This adaptation is strictly related to the method used for solving the boundary layer.

In Figure 5.4 the reader can see on the left hand side, that the boundary layer is modeled by reduced cell count method, which would correspond to a wall function approach. On the right, however, the boundary layer is resolved all the way to the wall by applying the inflation layer method. This method ensures the calculation of the boundary layer region for any wall-bounded turbulent flows. [4]
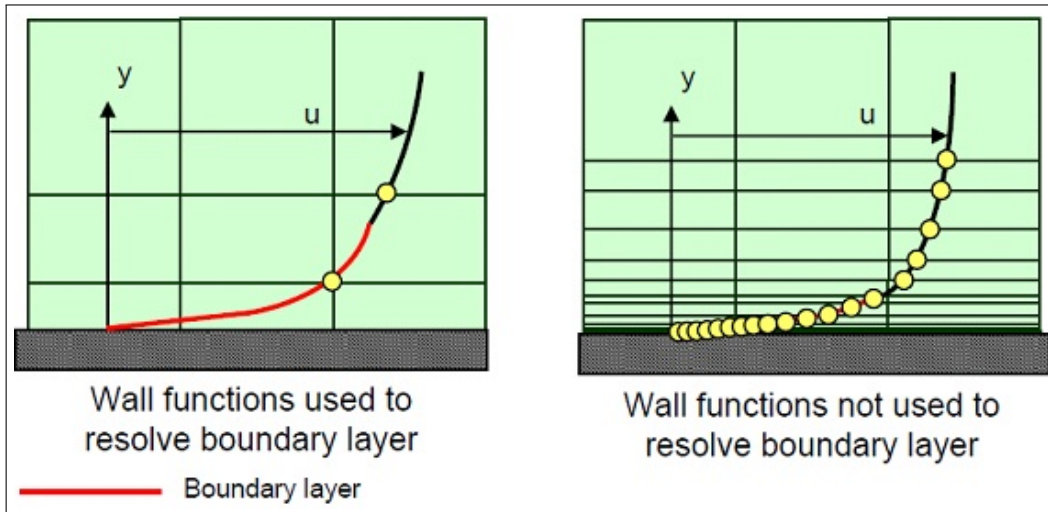
Figure 5.4: Representation of Wall Function approach vs fully resolving the boundary layer [4]

For solving our case, an inflation layer has been implemented on the extrados, intrados and winglets surfaces with a maximum of 5 layers and a growth rate of 1.2. The smooth transition option, which is the default one, has been applied to it. This option makes use of the tetrahedral element size in order to compute the local height of every element and their total height. In this way the volume change rate is made smooth. As each triangle inside the inflation layers will have an initial computed height with regards to its area, the initial heights will vary as we are in a not uniform mesh. [3]
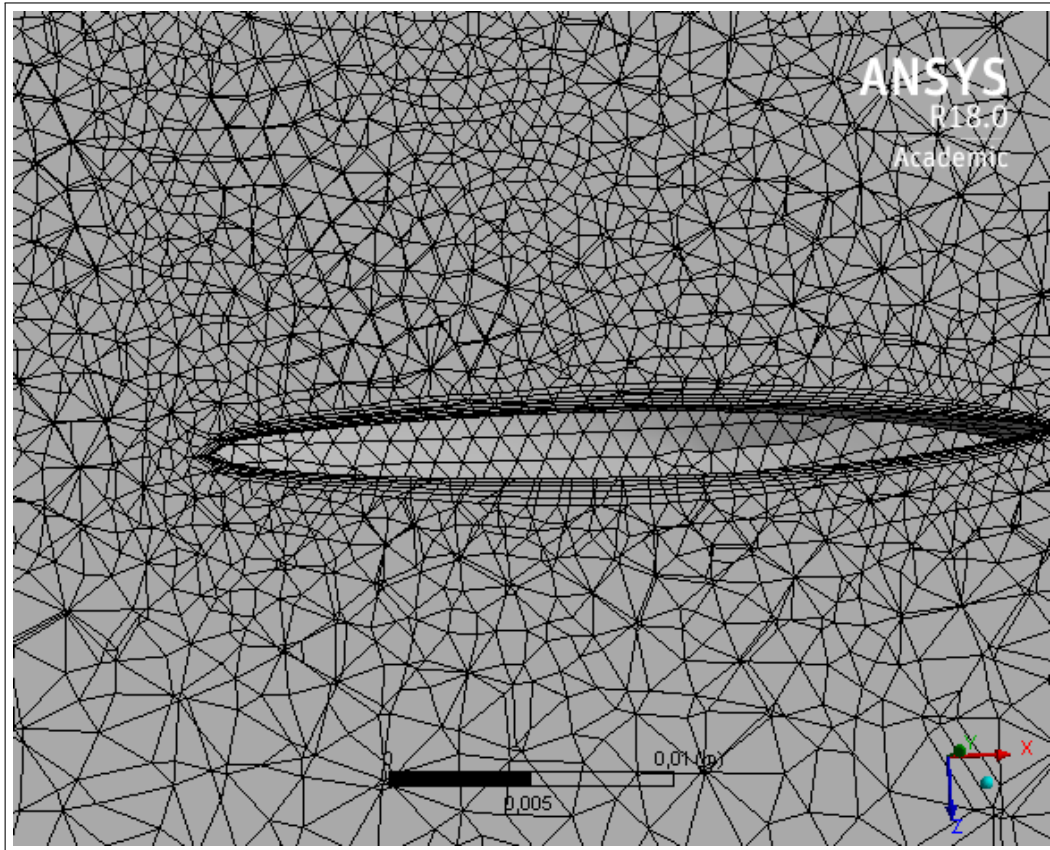
Figure 5.5: Example of Inflation layer on the blended winglet - section plane ANSYS

Once these options have been implemented, the mesh is generated. We can see two more captions of the mesh generated on the blended geometry as examples Figure 5.6. A section plane has been performed in order to show the cells distribution on the wing zone. If we center our attention on the first image, we can see a thick black line that surrounds the shape of the wing. This corresponds to the inflation layer that is also available on the wing. In image b) from Figure 5.6, we can see a wider view of the mesh. It is noticeable that the dark zones are corresponding to the wing and they present such color characteristics because the cell size is smaller there. It is also possible to check the tetrahedrons growth rate along the control volume.
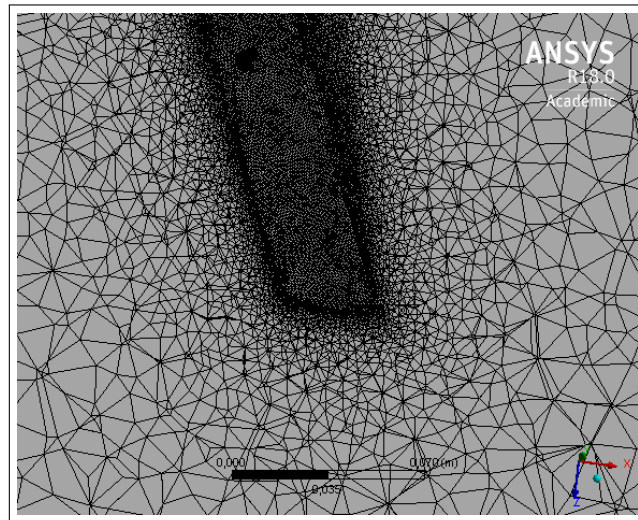
(a) Inflation layer on the wing
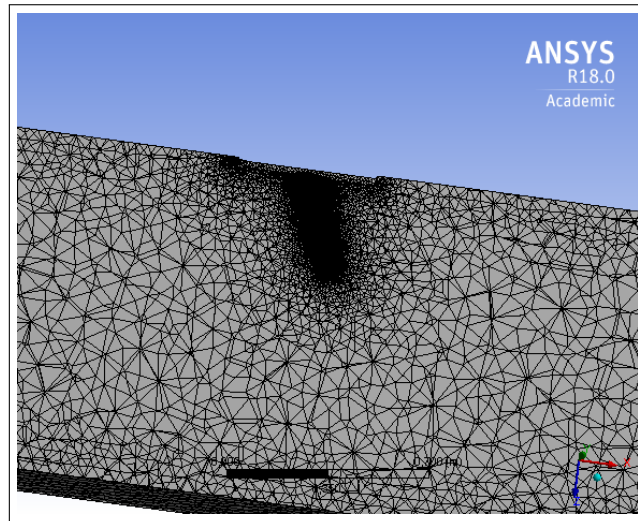
(b) General mesh layout

Figure 5.6: Meshing details overview - Section plane performed

5.3   ANSYS Fluent Set Up

In this section the flight conditions for our analysis will be presented along with the calculus method that we shall use in order to solve the problem. Cruise conditions are the most common conditions during the flight of an aircraft as it spends most of the time within this flight regime.

As mentioned before, the flight conditions for the A320 have been checked on the manual [22] and are indicated in Table 5.1.:

Flight Conditions (ISA Atmosphere)	
Height	37000 [ft] ($\approx$ 11000 [m])
Atmospheric Pressure	22632,04 [Pa]
Density	0.363918 [kg/m^3]
Temperature	216.65 [K]
MACH Num.	0.76 [-]
Angle of Attack	0 [rad]

Table 5.1: Flight Conditions

The next step is to choose the solver on the ANSYS Fluent software. While the pressure-based approach is usually used for low-speed incompressible flows, the density-based approach is mainly used for high-speed compressible flows which is the one we are studying in this project. With this approach, the momentum equations allow us to obtain the velocity field. The density field can be calculated by means of the continuity equation. Finally, in order to calculate the pressure field, the energy equation shall be used. This option shall be selected from the general Set Up options.

Before proceeding, it is of importance to state that in the first place, the mesh that was imported to fluent was 15.000.000 cells. In order to reduce the computational time, the polyhedra transformation was tried but it was still too large. This is why, as explained in previous sections, the average size of the used meshes is 2.000.000 elements.

As for the models, the energy equation has to be activated. Then, in or-

der to make use of the inflation layer we shall select the viscous model option from ANSYS Model list, which will augment the Navier-Stokes equations by adding a turbulence viscosity equation.

Following the explanation about the boundary layer made in the previous section when the inflation layer was introduced, it is important to remember that the flow near the wall can be divided in four regions as can be seen in Figure 5.7.:
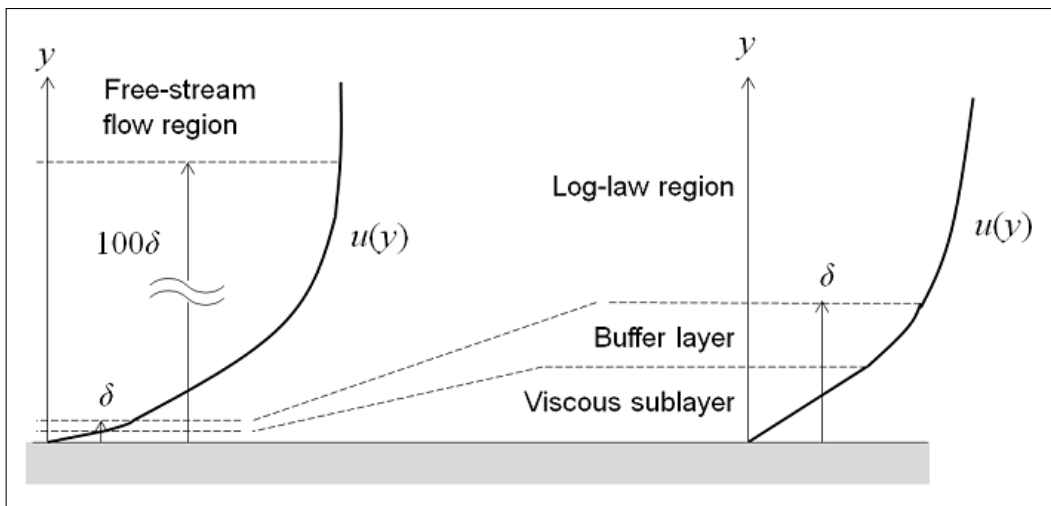
Figure 5.7: Four regimes of turbulent flow over a plane plate [8]

As presented in Figure 5.7., the fluid velocity next to the wall is zero. Just above it, a thin layer called laminar or viscous sublayer can be identified. As displayed on the enlarged view on the right, the average velocity function $u(v)$ is linear for the viscous sublayer. On top of this one, we can see the buffer region. In this area the turbulence stresses begin to overcome the viscous stresses and it will connect to a region composed by fully turbulent flow. This new region is defined as the log-law region as $u(v)$ behaves logarithmically. Last but not least, when we analyze the flow far from the wall, after the log-law region, we get to the free-stream section. In order to have an idea of the size of the layers, we can see that in Figure 5.7. that if we establish the distance to the end of the buffer layer as δ, the distance to the log-law region would be equivalent to 100δ [8].

In order to calculate how the flow behaves in its boundary layer, there are three main viscous models that have been considered for the resolution of each of the cases [8]:

- **Spalart-Allmaras**: This model adds only another variable for an undamped kinematic disturbed viscosity. This is a low Reynolds number model. It is important to bare in mind that the Reynolds number we are studying belongs to the fluid region close to the wall. This model does not compute in an accurate way those flow fields with shear flow or decaying turbulence. This is why, although it shows good convergence results we shall not choose this method for our calculations.

- **k-ϵ**: Two variables are solved by this method: k, corresponding to the turbulence kinetic energy; and ϵ, the dissipation rate of turbulence kinetic energy. This model calculates up to the buffer region, and it simulates the viscous sublayer flow. It presents problems when calculating adverse pressure gradients, strong curvatures to the flow or jet flows. Nevertheless, it performs well for external flow problems around complex geometries.

- **k-ω**: This third option is similar to k-ϵ as it is a low Reynolds number model. The kω model solves the flow for ω which is the specific rate of dissipation of kinetic energy. It is more nonlinear than the previous one. Thus, it is more difficult to converge. It is also sensitive to the initial guess of the solution and this means that an hybrid initialization must be performed before starting the iterative calculus. This model is more used for internal flows, flows that present strong curvatures, separated flows and jets. It can be considered the alternative model for Spalart-Allmaras.

For the very first calculus performed which was on the no-winglet geometry, the k-ω SST model was selected. This option combines both pure k-ω and $k - \epsilon$ models, erasing their weaknesses by complementing the free stream capabilities of the $k - \epsilon$ and the near-the-wall characteristics of k-ω. For this geometry the case could converge.

Nonetheless, when the other three geometries where implemented, the k-ω model was unable to converge even if the hybrid initialization was also

performed and then k-ϵ came to be the best option. Finally, from all the k-ϵ model options, the k-ϵ realizable was selected. This is because it is a newly developed model which contains new formulation both for the turbulent viscosity and transport equation for ϵ. The predictions provided are better than the ones we can get from the k-ϵ standard model, and it provides a better performance over complex surfaces such as the supercritical airfoil and the winglets geometries.

Concluded the models, the materials need to be selected. For the solid point of view, the default one (aluminum) is left as we are not interested in its mechanical behavior. As for the fluid, air is established as an Ideal Gas for its density calculation. As for its viscosity, the Sutherland law is applied. Due to this option, ANSYS Fluent can calculate the variation of air's dynamic viscosity as a function of temperature.

Afterwards, we shall set the boundary conditions. Thanks to the named selections generated in the Design Modeler stage, Fluent automatically generates wall boundary conditions (Stationary wall, no slip for shear conditions and standard roughness. There will not be any heat flux) on the fuselage, the intrados, the extrados and the winglet. It also applies the symmetry conditions to the symmetry plane.

The pressure far field boundary conditions set up deserves a special mention. There are several parameters that will need to be modified. In the first place, the Mach number needs to be set to 0.76 as suggested in Table 5.1. As there will not be any angle of attack, the Flow direction vector shall be [1 0 0]. Then, in order to set the altitude our plane shall fly in, both pressure and temperature must me input. Taking into account the values on Table 5.1, Gauge pressure shall to be set to a constant value = 22632.04 [Pa] and temperature will also be set as a constant value = 216.65 [K]. Both values have been taken from the ISA Atmosphere Table available in the Flight Mechanics class notes [20]. As for the turbulence intensity and viscosity ratio 5% and 10% shall be applied respectively.

Then, in the reference values section we shall load the pressure-far-field ones and both the area and the length need to be added in order to calculate the dimensionless aerodynamic coefficients.Thus, with regards to the area, we need to calculate the plane area of one wing which results in 62.81 [m^2].

Regarding the length, the mean aerodynamic chord is calculated and it results in 4.79 [m]. The graphical approximated methods used, can be checked in Figure 5.8 and they are explained in Flight Mechanics I class notes[21].
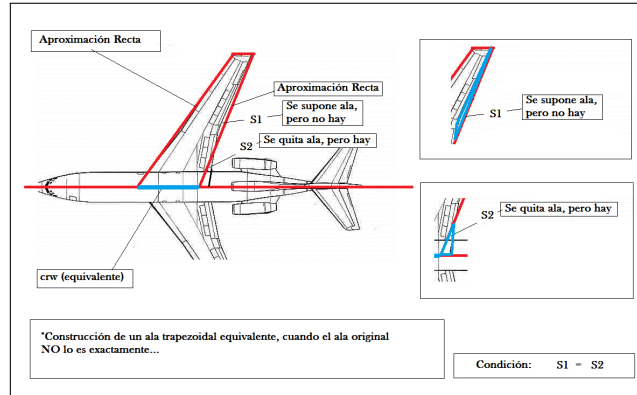
(a) Plain area graphical calculation

$$\overline{C} = (2/3)\, C\text{ root}\, (1 + \lambda + \lambda^2)/(1 + \lambda)$$

$$\overline{Y} = (b/6)\,[(1 + 2\lambda)/(1 + \lambda)]$$
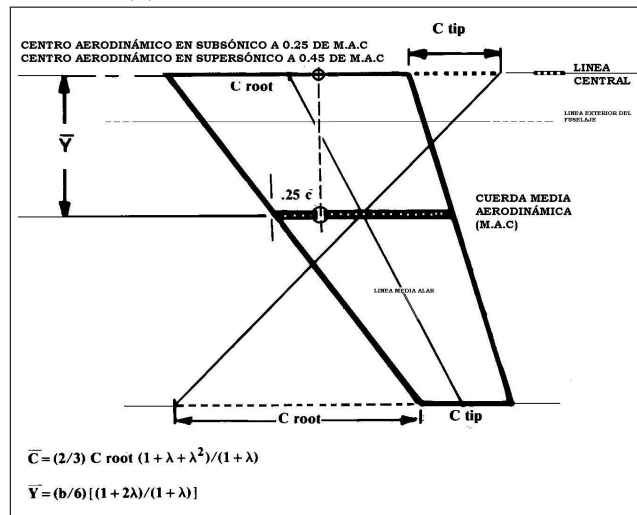
(b) Mean aerodynamic chord graphical calculation

Figure 5.8: Geometric parameters: Graphical calculation method [21]

Finally, we shall focus on the solution methods. As for the formulation, the implicit method will be left as default as well as the flux type options. As for the spatial discretization, the momentum, the turbulent kinetic energy and the turbulent dissipation rate will be solved by second order upwind

methods.

There is one more important parameter that can be modified. This parameter is known as Courant number and it is related to the Courant - Friedrichs - Lewy (CFL) condition. It is set as 5 and it can be reduced in order to improve convergence. The Courant number is related to the movement of the fluid through the computational cells. If it is ≤ 1 then the fluid particles move from one cell to another within one time step while if it is >1, fluid particles move through more than one cell at a time step. This decreases the computational time needed but can negatively affect the convergence [13]. Before switching to the k-ϵ method, the Courant number was reduced, but it did not solve the issue.

In order to check convergence, all residual monitors have been set to 0.001 and reports of the drag, lift and moment coefficients shall be launched. This has helped to evaluate the effectiveness of the Set Up and to keep track iterations development.

6

Processing

The domain and physical restrictions are already set. The next step is to run the calculation. In order to make the procedure lighter for the computer, Fluent will be launched with the 8 available processors put in parallel configuration.

In addition to this, before proceeding with the iterative method it is important to check the scaling factor, as we used the escalated model for building the mesh, now the scaling factor applied will be of **50:1** in order to come back to real dimensions. We also need to make sure we are in steady state conditions and with velocity formulation set as absolute. It is also important to check that the units are the ones of the International System. Once these routine steps are performed, another good idea is to check the mesh and try to improve its quality. As the control volume is so large, there will be elements far from the airplane geometry that might present issues with their orthogonality quality. There are some cells that present values lower than 0.5 in all four cases. By setting the improve grip quality option, this minimum value can be improved significantly.

Once these parameters are checked and both solution methods and solution controls are set as explained in the previous section, it is time to initialize

the calculation. There are two main ways for initializing the calculation. The one we shall launch will be the Hybrid option.

As for the characteristics of this method, the hybrid initialization, as explained in the ANSYS Help Viewer, is a collection of recipes and boundary interpolation methods. It can solve Laplace's equation in order to produce a velocity field that adapts to complex geometries and a pressure field that connects high and low pressure values in a smooth way. One main asset is that the other variables shall be patched based on domain average values or a predetermined recipe.This means that its set up is more or less automatic and it is the software which manages it.

Finally we can run the calculation. During the iterative process, an important issue appeared aside from the non-convergence problem explained before. Although the mesh quality was improved, in some cells the turbulent viscosity was limited to viscosity ratio of 1.000000e+05. This happens at the the outlet and the inlet as the quality of the mesh in those regions is the poorest. This problem appeared on nearly the 0.001% of the cells in each of the four cases. Although it does not mean a big deal towards the accuracy of the results obtained and indeed, convergence is achieved, it gives a hint on how initially the turbulence intensity is too large.[6]

Finally, the cases converged on an average time for completing the computations of 10 h each so that the residual monitors could reach the absolute criteria of convergence $= 10^{-3}$.

7

Post processing

ANSYS Fluent allows the user to gather both numerical and graphical data. Thanks to the CFD analysis, it is possible to get images that show a complete map of the variables values distribution which is really useful when trying to check the influence of variable geometries, as we are doing through this project. It also outputs a complete report of those variables of interest, which in our case would be the aerodynamic forces and their dimensionless coefficients.

For this project both results formats will be used in order to compare in full detail all the important values calculated.

With regards to the numerical reports, which will be presented on the next section, they can be launched from the Forces Reports option of ANSYS Fluent. It allows to print on the console the values per each of the named surfaces that generate those aerodynamic reactions which are the fuselage, intrados and extrados. It is possible to get them as a vector of 3-dimensions, where x coordinate will be axial force, y will be the normal force and z will be the side force. As we have 0 rad angle of attack, drag force will correspond to the axial force (positive sense) and the lift will correspond to the normal force (positive sense). These reports also present the calculated coefficients.

They are deduced using the geometric reference values that were presented in subsection 5.3.

Focusing now on the graphical reports, they present a rated variation of values over the selected geometries which shows the changing variables over the surfaces. In order to gather information about how the flow behaves outside the geometry, some tool geometries must be designed and implemented. It can be done by using FLUENT create tool.

This strategy will be useful for checking variables such as static pressure, Mach number, vorticity or turbulence intensity. Those will be the main factors that the graphical study will present. They will help to compare how the winglets affect the pressure difference between the intrados and the extrados of the wing or the turbulence generation at the wingtip. They will also help to locate the generation of potential shock waves. In order to do so, the extra tool planes will be placed in three important places: on the wingtip, cutting the winglet; next to the winglet, where its rood appears and on the middle of the wing, in order to check if the winglet influence gets far from the wingtip or if it gets diluted.

From all the options available, such as pathlines or vectors, the most representative one will be the contours. Due to some limitations in the hardware available for the processing of such data, contours will be the most feasible option as they will imply less computational effort than the other options. In addition, vectors and pathlines can be useful if the images are taken from a very small and specific area, which in our case is not so interesting for the purposes of this project.

One last comment must be done. In order to be able to compare using the colored contours, we shall use the same scale for all the Static Pressure contours. This procedure will be also applied to the Mach number, vorticity and turbulence intensity contours.

8

Results

After all the Set Up is arranged, the calculus are launched and the data is gathered, it is time to analyze the outcomes. For this purpose we shall compute both numerical data with the help of several tables and graphical data by means of screen-shots performed by ANSYS Fluent assistant.

8.1   Numerical results

The reports presented by Fluent show 3 coordinate vectors corresponding to axial, normal and side forces. We are only interested in the two first as they correspond to the Drag and the Lift forces because the angle of attack is α = 0°, whose variations depending on the geometry configuration are the aim of study for this project. Thus, the tables presented in the following pages will show 2D vectors. The first coordinate corresponds to the axial force and the second coordinate will correspond to the normal force.

It is also important to check the value of Reynolds number. Reynolds number ratio compares the inertial resistance over the viscous resistance for a flowing fluid. The Reynolds number is mostly used for checking the flow

characteristics. A fluid flow that presents low Reynold numbers will be governed by its viscosity features. A low Reynolds number means that the flow is steady, viscous or laminar. For high Reynolds numbers, our flow will be turbulent, and the momentum of the fluid will be more important than viscosity when it comes to describe its nature.

Reynolds number equation is as follows:

$$Re = \frac{vl}{\nu} \qquad (8.1)$$

Being:

- v [m/s], the free stream velocity;

- l[m] the mean aerodynamic chord width;

- ν[m/s^2], the kinematic viscosity of air at our flight conditions.

For our particular case, far from the walls, the Reynolds number will be high, ($Re = 101,256,541$) as the free stream velocity is near the sound speed. Nonetheless, the zone we are interested in is the zone close to the wall, defined by the boundary layer. In this zone, the velocity will be low, and therefore the Reynolds number will be also low, making viscous effects becoming really important.

8.1.1   No winglet geometry

In this subsection the results reported by ANSYS over the geometry without winglet are presented. As we can see the output aerodynamic coefficients are presented in several columns, in order to separate the pressure-based coefficients from the viscous-based coefficients.

Aerodynamic Coefficients: no winglet geometry			
Coefficient	Pressure-based [-]	Viscous-based [-]	Total [-]
Lift Coefficient	0.31174621	-6.187e-05	0.31168434
Drag Coefficient	0.092454724	0.006103	0.098557786

Table 8.1: Aerodynamic coefficients: no winglet geometry

In table 8.1 we can see the values for the two aerodynamic coefficients. As we can see, both pressure and viscosity contribute to both lift and drag coefficients. On the one hand, we can see that in the CL (Lift Coefficient) case, viscosity affects reducing the Total value. On the other hand when talking about CD (Drag Coefficient), viscosity increases it, which will therefore increase the aerodynamic resistance.

Then, as we already stated several times, this project will be centered on the induced drag, which corresponds to the pressure-based Drag coefficient which, as we can see on the table is higher than we could expect on a usual wing. This can be attributed to the 3D-Flow effect on the wing. As there are no wingtip devises, the flow interference from the intrados to the extrados the upper surface is not controlled, and therefore the aerodynamic resistance is increased. With regard to the lift coefficient, it is lower than the value we could usually get. This is due to the supercritical airfoil that has been implemented. The lift generation is restricted to the rear part of the section, where the curvature is increased, as explained in section 3.2.

We shall take these values as the foundation for comparing them to the rest of geometries in order to review all the pros and cons that the other configurations imply.

8.1.2   Raked winglet geometry

Following with the analysis, the first geometry we shall face is the raked geometry. As explained in previous sections, this wingtip device increases the effective aspect ration of the wing by increasing the wingspan. This increment will also mean a growth on the wing surface and therefore we should see an increase of the lift generation with respect to the first case. As it partially interrupts the wingtip vortexes generation, it will also reduce the induced drag experienced by the airplane.

Aerodynamic Coefficients: Raked winglet geometry			
Coefficient	Pressure-based [-]	Viscous-based [-]	Total [-]
Lift Coefficient	0.3842515	-4.994e-05	0.38420156
Drag Coefficient	0.042420095	0.0072857119	0.049705807

Table 8.2: Aerodynamic Coefficients: Raked winglet geometry

As we can see in the table 8.2. both predictions were right. The reduction of the total drag coefficient with respect to the first case is of a 49.59%. This configuration increases a 23.07% the lift generation over a wing configuration without any wingtip devises.

In terms of viscous effects, it is interesting to see how having extra surface increases the viscosity contribution for both CL and CD in comparison to the values obtained for the non-winglet case.

With regard to the pressure-based coefficients, we can see that the drag coefficient, which will be the induced drag has suffered an important reduction, as the total value. This fact demonstrates that although there is an increase in the viscous drag, due to the larger surface of the wing, reduction on the induced drag is much bigger and therefore it is worthy to implement this kind of winglet.

It is therefore visible how much can the 3-D Flow interference between the intrados and extrados affect to the general performance of the wing.

From the value of the total CL the total Lift can be calculated with the following formula:

$$L = \frac{1}{2} \, \rho \, CL \, A \, V^2 \; =$$

$$= \frac{1}{2} \; \times \; 0.363918 \; \times \; 0.38420156 \; \times \; 125.62 \; \times \; 224,25244^2 \; = \qquad (8.2)$$

$$= \; 441637.3636 \; [N]$$

This value can also be obtained from the ANSYS Forces report. we can see that the lift generated with both wings is lower than the weight of an A320 (755112,05 [N] for max. takeoff weight) [7]. This basically means that the airfoil chosen for this project is not the one that Airbus implements on the A320, as they need to generate more lift than we do, with the same wing geometry (surface and shape). This phenomenon is also applicable to the rest of winglet geometries.

It was expectable that the lift generated would not match the A320 real specifications, as we never had the information related to the A320 airfoil configuration. This matter will not affect to the conclusions of this project but it is a remarkable aspect that was singular enough to be pointed out.

8.1.3   Blended winglet geometry

The next geometry to be analyzed is the blended winglet. This geometry is commonly used by Boeing on their 737 models. As explained in previous sections this configuration improves the payload/range capability of airplanes instead of improving fuel consumption. Having more available range is an important asset for B737 class aircrafts as they perform continental flights. It also improves the engine performance which is directly linked to a reduction on their maintenance costs. It increases the optimum cruise altitude as well. This will mean an improvement on the overall flight performance and drag generation [26, see].

In table 8.3. the reader can observe the values calculated for the blended configuration:

Aerodynamic Coefficients: Blended winglet geometry			
Coefficient	Pressure-based [-]	Viscous-based [-]	Total [-]
Lift Coefficient	0.39743348	-4.8892585e-05	0.39738458
Drag Coefficient	0.043341743	0.0073661248	0.050707868

Table 8.3: Aerodynamic Coefficients: Blended winglet geometry

The results obtained are the ones expected and they show us some interesting aspects of Boeing's design and manufacturing strategies.

With regards to the drag generation, there is an decrease of 48.58% with regards to the no winglet configuration, whereas there is an increase of 2.01% with regards of the raked winglet geometry. When focusing on the lift generation, this geometry is going to be the best one of the four cases studied, with an increase of 27.24% with respect to section 8.1.1 case and an increase of 3.39% with respect to section 8.1.2.

If we now focus on viscous vs pressure coefficients, we can see that the contribution of the viscosity is really similar to the one provided by the Raked winglet. With this in mind, it is possible to point out that the induced drag by the Blended case is bigger than the one induced by the Raked configuration, as we can see if we compare tables 8.3 and 8.2. Additionally, the CL is also higher, which will bring a larger Lift generation.

We can see, as we explained at the beginning of this section, that the viscous effects on a macro scale do not affect significantly the overall values. As we will see later on, they will be very important close to the wall though.

These values sustain the real strategies applied by Boeing. While raked wing tips are more efficient in long cruise phase segments, blended winglets are more efficient in climb phase. This is why raked winglets are being implemented in bigger planes such as B747 where the cruise phase optimization means a greater range and significant less fuel consumption whereas blended

wingtips are included on those smaller aircrafts that perform shorter flights. These smaller airliners perform a higher number of climb and approach segments. Those phases also represent a bigger percentage of flight total range in B737 than in B747 and this is why a big percentage of the fuel consumed is linked to the aircraft performance on these segments [16].

8.1.4   Endplate winglet geometry

Last but not least, the Endplate winglet is the next geometry to be studied. Overall, it could be said that Endplate and blended configurations are similar on the first glance. They both increase the wing's height and therefore they both move the vortexes origin far from the wing surface. They also present a vertical sweep angle whereas Raked winglet sweep angle is horizontal.

Finding more similarities, Endplate winglets are the option chosen by AIRBUS for their A320 series aircrafts. This airliner's performance could be said to be equivalent to the B737 as they usually deal with the same kind of continental flights. This means that while Boeing developed the blended geometry for their short-flight aircrafts, AIRBUS bets on the Endplate winglets for getting similar outcomes on the improvement for climb and approach phases.

AIRBUS has also implemented the Endplate devise on the A380 airplane, but it is combined with an horizontal change of the sweep angle, so it looks like a combination of a raked plus endplate winglet. Taking into account the characteristics seen up to now it can be inferred that this combination aims to improve the climb and approach phases with the endplate geometry and the cruise segment with the "raked transition" between the wing and the wingtip.

All in all, in table 8.4. we can see the aerodynamic coefficients values for the Endplate winglet:

Aerodynamic Coefficients: Endplate winglet geometry			
Coefficient	Pressure-based [-]	Viscous-based [-]	Total [-]
Lift Coefficient	0.35273417	-6.1244646e-05	0.35267293
Drag Coefficient	0.042000862	0.0064239416	0.048424804

Table 8.4: Aerodynamic Coefficients: Endplate winglet geometry

Following the tendency established by the previous two wingtips, thanks to the Endplate configuration the total drag is reduced in a 49.59% and the total lift generation is improved by 13.14% with regards to the wing with no wingtip devise.

Comparing the values presented on table 8.4 to tables 8.1, 8.2 and 8.3, we see that with respect to the raked winglet, total drag generation is reduced in a 2.62%. Similarly the overall CL is a 8.07% lower. As for the blended winglet, total drag is reduced in a 4.54% and total CL is also reduced by a 11.08%.

When talking about viscosity effects on the aerodynamic coefficients, the Endplate winglet produces similar values for both CL and CD to the ones generated by the no-winglet case.

The results on table 8.4 highlight the fact that this configuration is good with regards to the induced drag reduction, as we can see on the Pressure-based Drag coefficient cell (as well as on the Total CD cell), but the lift generated is way lower than the other two winglet configurations.

These values allow us to answer the question raised in section 3.1: Is it true that for the Endplate to be 100% effective, the surface should increase so much that skin friction would generate a larger drag force than the reduction of induced drag obtained? The answer is that it is certainly true that in order to get a lift equivalent to the Raked or Blended winglets, a bigger surface should be implemented. This of course would mean an increase in the viscous contribution to the drag coefficient. Nonetheless, the main aim of the Endplate winglet is not to generate as much lift as the Blended or the Raked, but to reduce in a bigger percentage the Induced Drag. Therefore, there is no need for bigger surface, as the primary goal is accomplished already.

Summarizing, we can say that blended winglets are more efficient and evolved than Endplates when it comes to lift generation. This is historically reasonable as Endplate winglets where successfully implemented for the first time in 1910 [25] by William E. Somerville while blended winglets were developed by Boeing in the 1990s by Aviation Partners [16].

8.2   Graphical results

Once the numerical data has been presented and analyzed, it is time to check, visually, how flow behaves over the wing. Throughout this section, several contour images will be presented. This option has been chosen, as explained in the previous section because it provides a good overall view of the flow state. These images have been auto-ranged in order to have a proper scale of values that will help the reader to understand the code of colors and to understand the order of magnitude we are working with.

It is important to keep in mind that the CFD analysis which handles these colormaps by solving the Navier-Stokes equations is subject to the accuracy of the mesh developed, which is subject to the computational power of the computer. This means that the separation between isopressure and isoturbulence lines might not be as precise as it could be in an industrial environment. Nontheless, it will be enough for the comparative mesurements we are handling.

As it has been done on the previous section, several subsections will be presented below in order to work over all the configurations.

8.2.1   No winglet geometry

The no-winglet geometry is the basic configuration. In Figure 8.1. it is possible to observe a 3D-View where the distribution of the static pressure on the extrados is mapped. At 1/4 of the chord there is a drop of pressure which is more intense at the wingtip. This drop of pressure provokes an acceleration

of the flow. We can see how the pressure values stay approximately constant until the Trailing Edge, where the increase of curvature characteristic of the supercritical airfoils is placed.
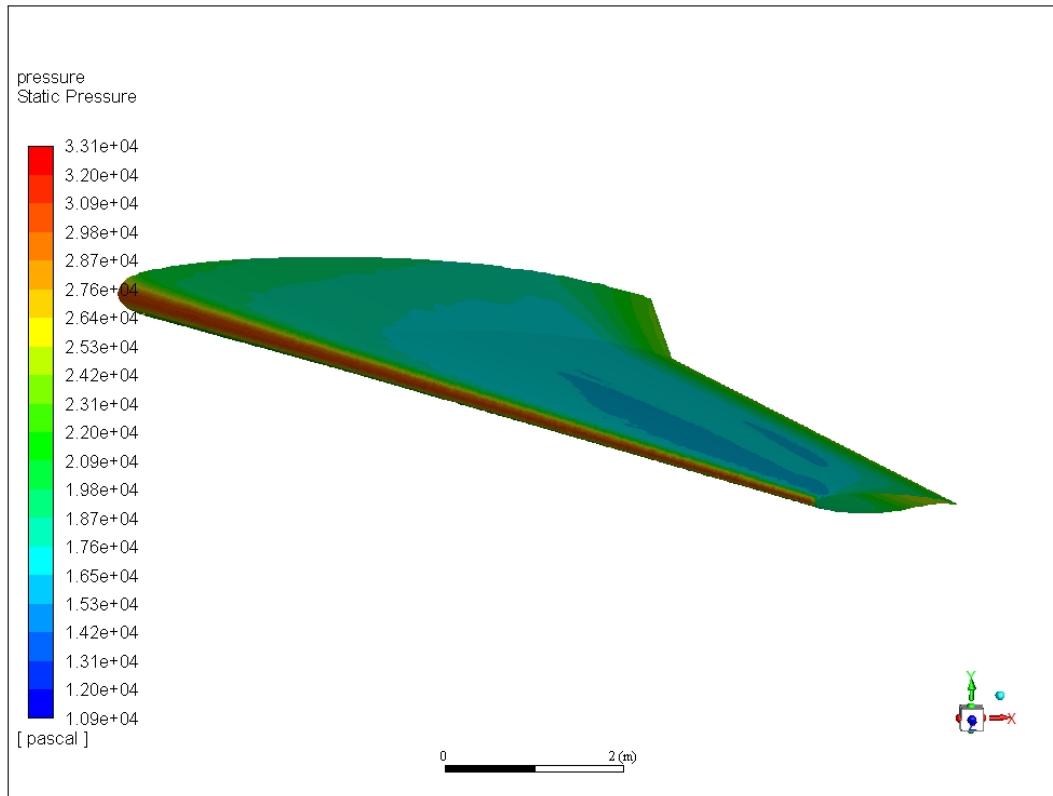
Figure 8.1: Static Pressure 3D-View over the wing surface: no-winglet configuration

Thanks to Figure 8.2., it is possible to see the Static Pressure contours at the wingtip. It is possible to observe how the pressure drops on the extrados getting lower values than the pressure in the intrados, near the 1/4 of the chord. Despite this, due to the airfoil's thickness, the contribution to the lift generation of this pressure difference is relatively small. The main source of pressure difference can be located near Trailing Edge, where the curvature increases in the intrados. This characteristic feature of such supercritical airfoil makes the static pressure value on the intrados to increase notably in comparison to the rest of the intrados pressure distribution. The difference

in pressure between intrados and extrados will be therefore greater and a bigger amount of lift will be generated.
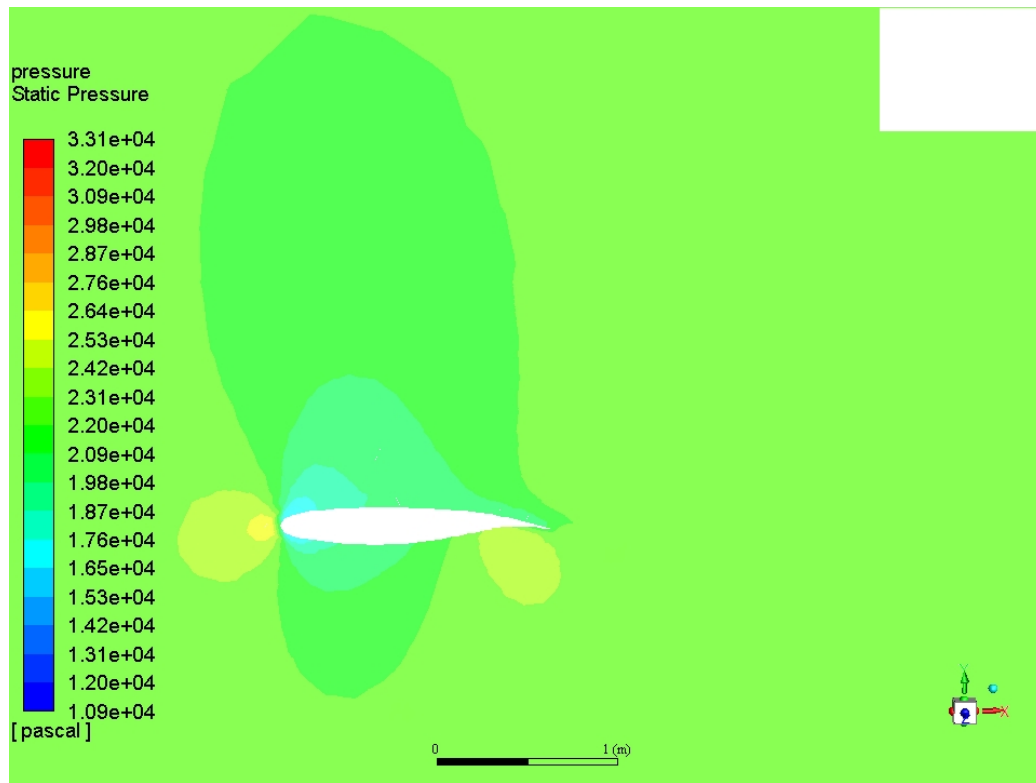
Figure 8.2: Static Pressure distribution over the wingtip airfoil: no-winglet configuration

Another point to be highlighted is that as the pressure drops when getting closer to the trailing edge, it should come back to the free-stream pressure values. However, this does not happen immediately after the trailing edge's end. In order to know more about this transition area, more data will be needed related to the turbulence intensity and vorticity magnitude. This data will be presented in Figures 8.5 and 8.6.

In Figure 8.3, the reader can see another static pressure contour. It corresponds to a cut performed in a point between the wingtip and the wing root, in order to avoid both zones' interference. As we can see, the shape of

the pressure contours is as expected: some pressure drop at 1/4 of the chord and a major pressure difference near the TE. What is important to notice is that the pressure distribution is now more homogeneous on the extrados and the increase of pressure due to the increase of curvature at the intrados near the TE is more intense. The difference between Figure 8.2 and 8.3 shows that the interference of the 3D flow from the intrados to the extrados trully affects the pressure distribution and therefore the Lift and Drag generated.
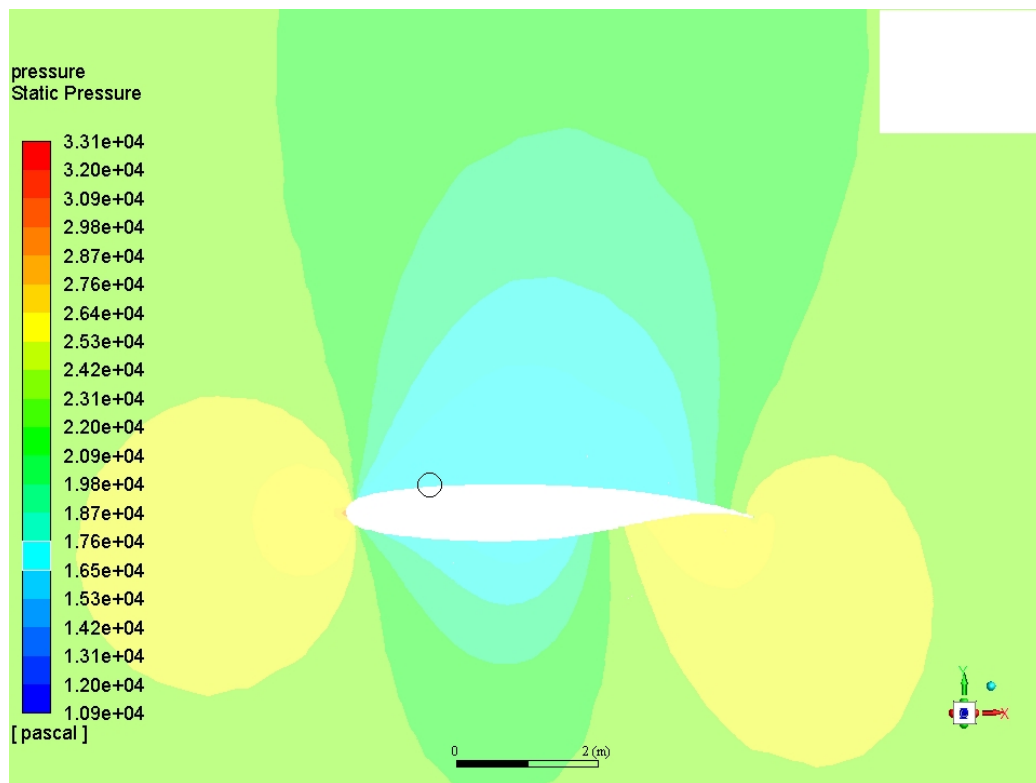
Figure 8.3: Static Pressure distribution in the middle of the wing - no winglet Geometry

We can also see in both Figures 8.2 and 8.3 that no shock wake seems to be generated. In order to be certain of this information, we can check hot the Mach number variation over the airfoil behave in Figure 8.4. It that Figure it is possible to observe that the Mach number on the extrados is accelerated up to M=0.94 at 1/4 of the Chord and then it drops down to approximately

M=0.76 which is located in the big and long green wake. If we focus on the circle marker, just next to the airfoil's end, M is lower than the free stream Mach number. This phenomenon is due to the vorticity which can be spotted on Figure 8.6.
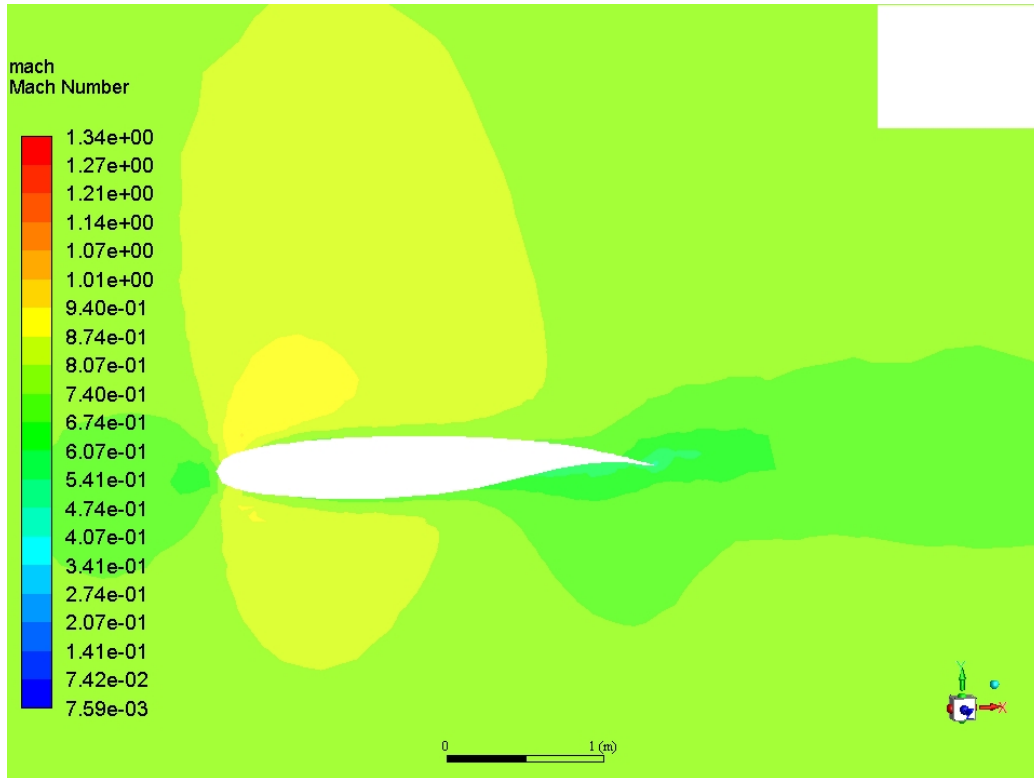
Figure 8.4: Mach number distribution over the wingtip airfoil: no-winglet configuration

On Figure 8.5, the turbulence intensity colormap is presented. Firstly, we can spot a thin layer surrounding the airfoil which is the boundary layer. This layer, as shown in the Figure, is turbulent. This information is consistent with the statement made at the beginning of this section, where it was suggested that a low Reynolds number would be encountered in this area of the flow, due to the low speeds present near the wall.
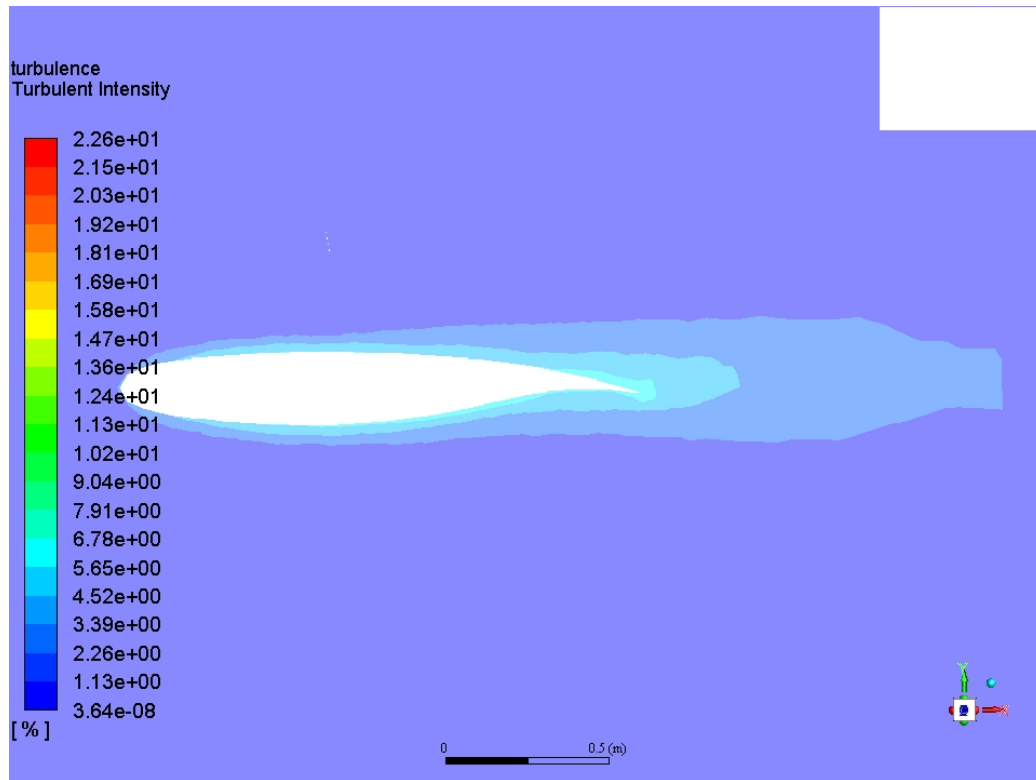
Figure 8.5: Turbulence intensity contour at the no-winglet's wingtip

The layer thickness increases as it looses energy, blurring the lines into the free stream flow conditions. This behavior will affect negatively the lift generation in this rear part of the airfoil and it will increase the drag generated. In order to know if the layer detaches from the airfoil's surface, it will be necessary to check the vorticity magnitude contour, as shown in Figure 8.6.

By using ANSYS Polyflow, we can calculate the vorticity vector and get a distribution of its magnitude. Vorticity is defined in in formula 8.3, as the curl of the velocity vector and it is the measure of the rotation of a fluid element as it moves through the flow field.

$$\xi = \nabla \times v \tag{8.3}$$

In our 3D case, it appears as a vector in the postprocessing graphical output. This is why it is represented by the contours of this vector's magnitude.

All in all, we can see in Figure 8.6 that there exists a small zone where some vorticity is generated. This vorticity explains the low Mach values encountered in Figure 8.4, but it is not strong enough to make the boundary layer detach from the airfoil's surface.
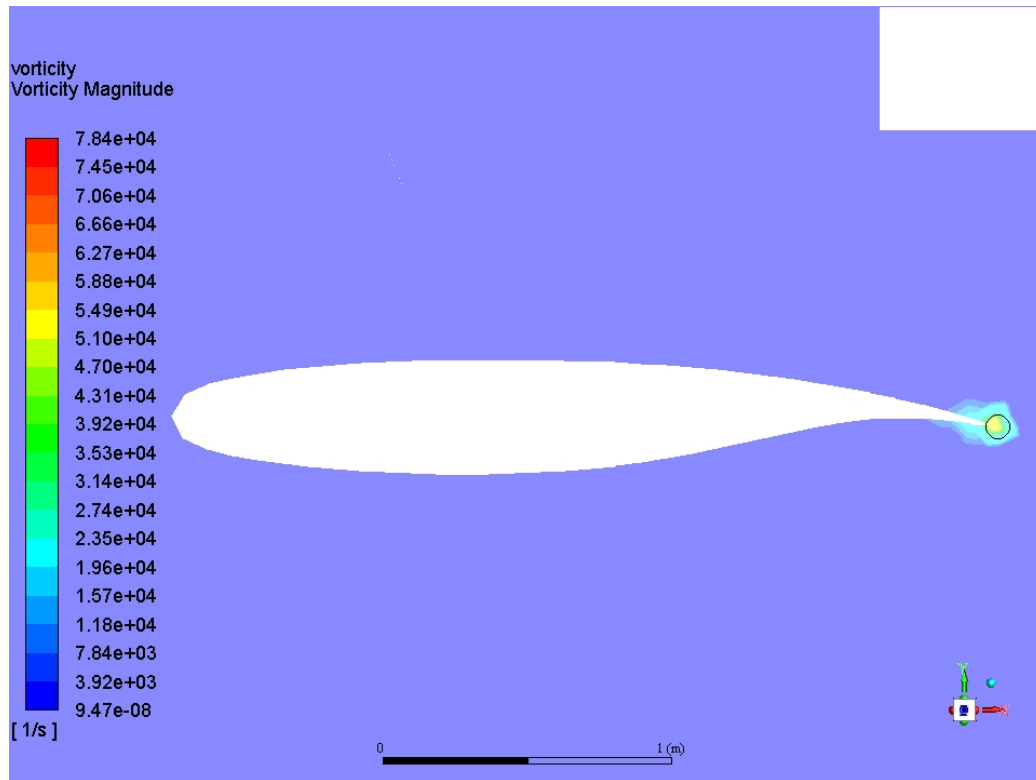
Figure 8.6: Vorticity magnitude contour at the no-winglet's wingtip

It is important to highlight that on the bottom of each figure a rule can be found where the scale can be seen. It is remarkable that this wake can be measure more than 2.5 [m] long in cruise conditions. Such situation when taking off will be incremented by the floor interference, the bigger density value of the air and it explains how much the flow can be perturbed. This is why Airport Traffic controllers must leave some time between take-off or landing operations, as it can strongly affect the plane behind generating strong downwash flow disturbance.

8.2.2   Raked winglet geometry

After facing the previous case, now we shall analyze the Raked geometry. In the Figure 8.7, a general 3D overview of this case is presented.

When comparing this 3D overview with Figure 8.1, it is possible to see that the pressure drop this Raked winglet configuration shows is greater than the one happening on the no-winglet case extrados. This strong drop represented in dark blue starts as soon as the sweep angle from the Raked winglet is equal to the wing LE sweep angle. It is important to see that there is also a small drop of pressure on the winglet extrados, which potentially means that it should be fostering the lift generation at the wingtip, which was not happening on the no-winglet case.
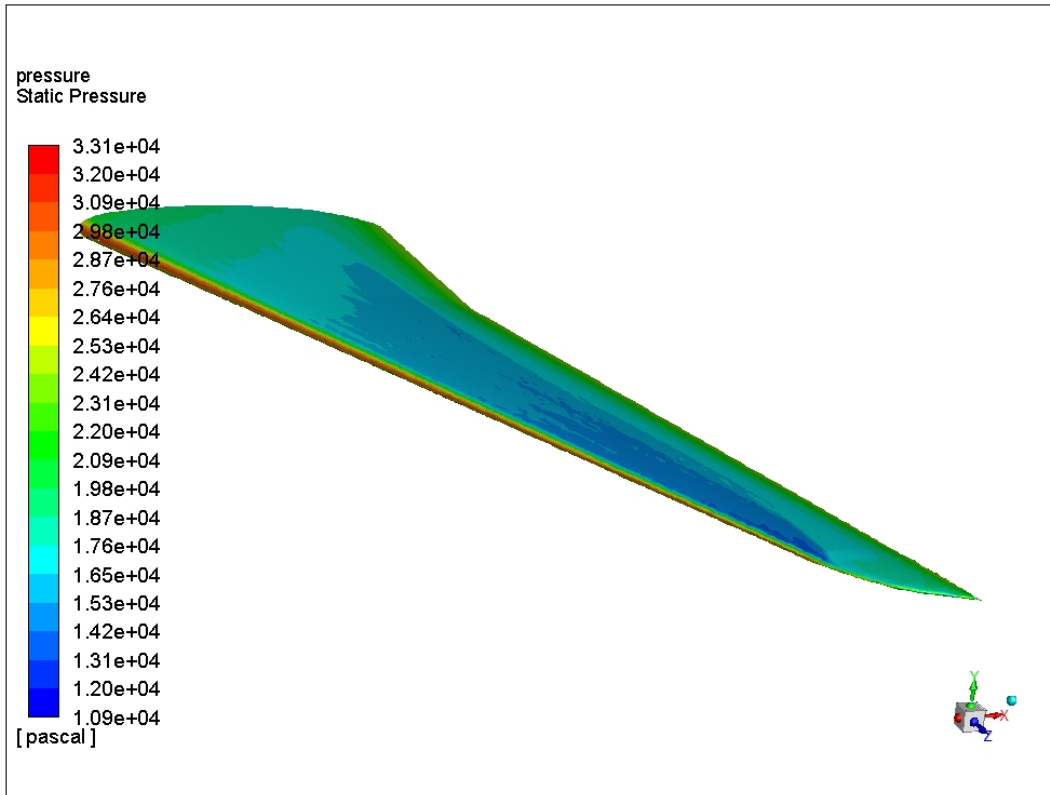
Figure 8.7: Static Pressure 3D-View over the wing surface: Raked configuration

At a first glance we can see thanks to Figure 8.7 that this configuration shall generate greater pressure differences between the intrados and the extrados, resulting in a bigger lift generation.

The Figure 8.8 shows the static pressure contour associated to this geometry. As in the previous case, the plane was placed at the wingtip, this new vertical plane, which helps us to print the contours, is located at the raked winglet root, i.e. where the sweep angle of the LE starts changing. That is the equivalent position to the no-winglet vertical plane on the wingtip. By placing both planes approximately on the same spot, it will be possible to compare the effect of the winglet on the same airfoil and therefore the results can be more representative.

In comparison with the no-winglet configuration, we can witness that the acceleration of the fluid will be greater. The same isopressure levels appear in both Figure 8.2 and 8.8, but in this last one, they are larger. Another interesting factor is that this pressure distribution looks very similar to the one shown in Figure 8.3. It is important to highlight that whereas Figure 8.3 shows the pressure distribution in the middle of the wingspan, this Figure 8.8, shows it at the beginning of the Raked Winglet. We can conclude due to these contours that this device effectively disrupts the interference from the intrados to the extrados.
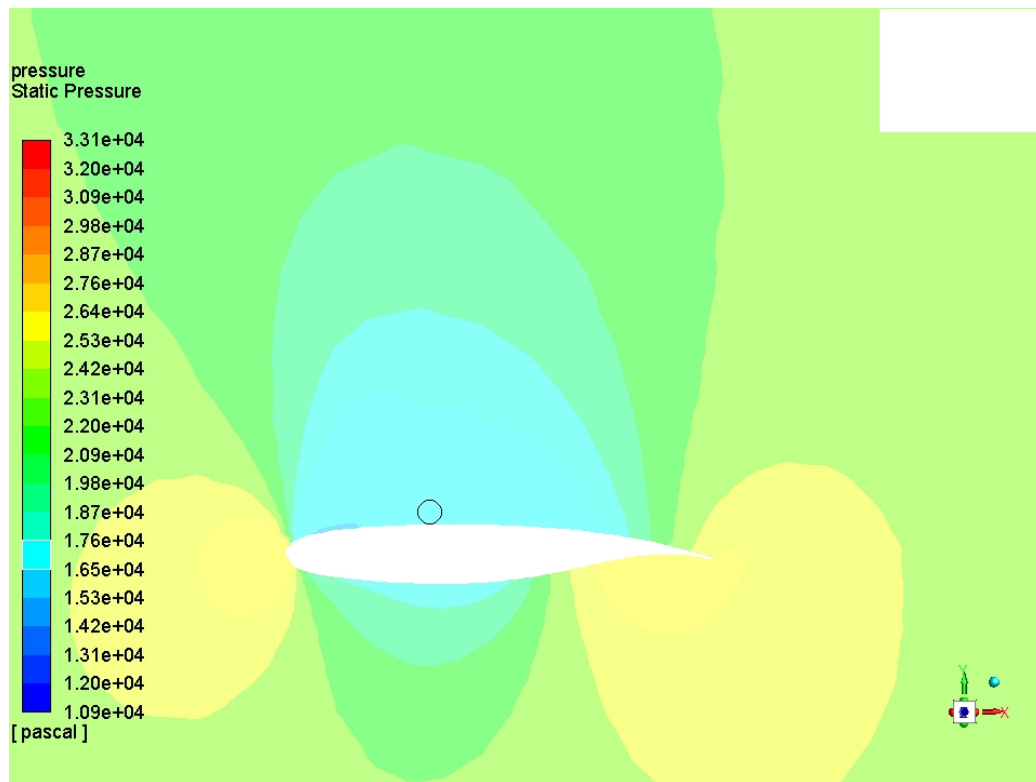
Figure 8.8: Static Pressure distribution over the airfoil placed before the beginning of the Raked winglet

As in Figure 8.3, Figure 8.8 shows a pretty homogeneous pressure distribution on the extrados and a big discontinuity at the intrados due to the curvature change.

If we now focus on Figure 8.9, which represents the Static Pressure distribution in the middle of the wing, we can see that both Figure 8.8 and 8.9 look very similar. This means that an homogeneous pressure distribution over the wingspan is granted thanks to the winglet and therefore, we can notice in both that the values presented on the Numerical Results section make sense. Lift generation will be greater in the Raked case than in the no-winglet case.

Figure 8.9: Static Pressure distribution in the middle of the wing - Raked Geometry

In both Figures 8.8 and 8.9, it is not possible to locate any shock wave conditions. In order to be sure of this, Figure 8.10 shows the Mach number contours.

It is possible to spot an acceleration of the flor, near 1/4 of the chord, reaching values around M=1. Nonetheless, the deceleration of the flow seems to be smooth, no abrupt change in Mach number appears, so there are no shock waves generated.
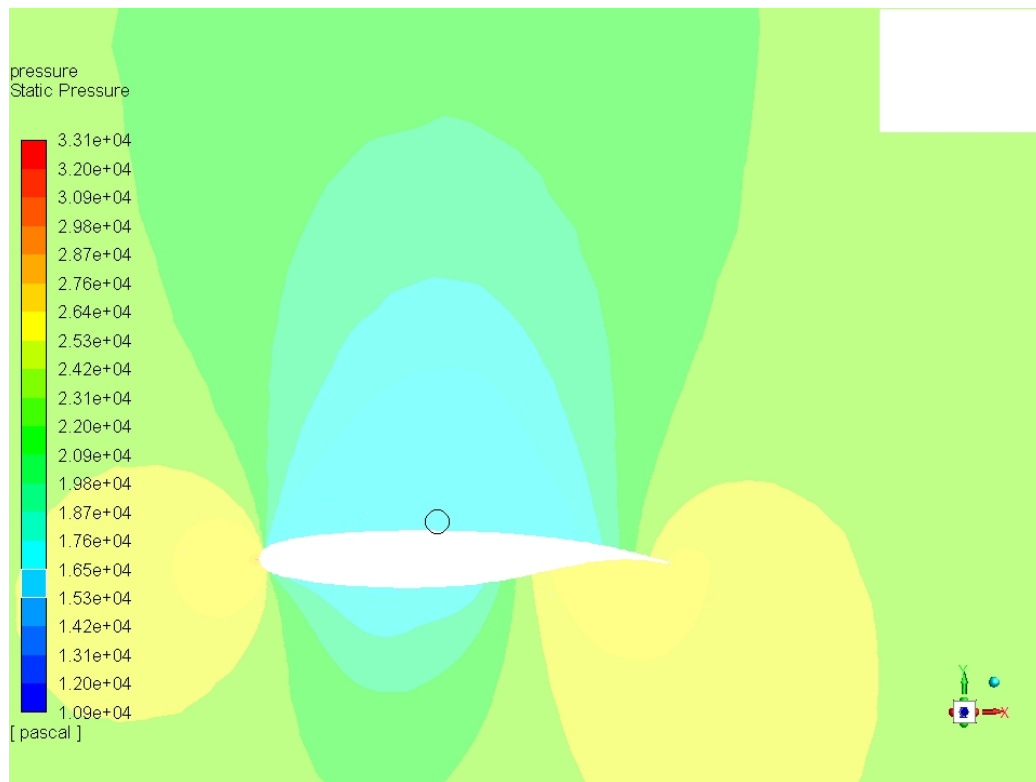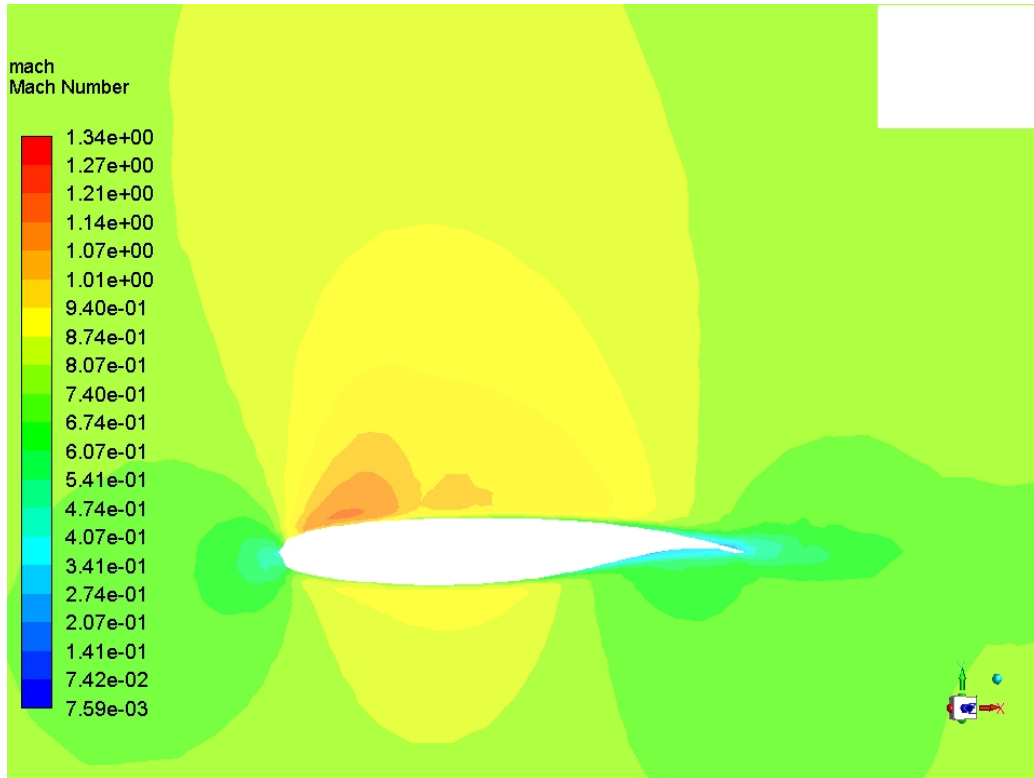

Figure 8.10: Mach number distribution over the airfoil placed before the beginning of the Raked winglet

Following with the analysis, we can now check the turbulence intensity generation. Figure 8.11 shows how the turbulent boundary layer is again generated and covers all the wing surface. A remarkable difference between Figure 8.11 and 8.5 is the change in the wake's size. As the winglet affects the lift generation, it inputs more energy into the boundary layer which allows it to remain thin for more distance than in the no-winglet case. This will suppose an important reduction of the drag force and it will help to the lift generation and the wake will be smaller and weaker.

Last but not least, Figure 8.12 shows us the vorticity magnitude. It is not possible to appreciate great changes in the contours. This brings us to the conclusion that the raked winglet avoids in a great measure the vorticity generation which is a consistent fact with all the previous data presented for this case.
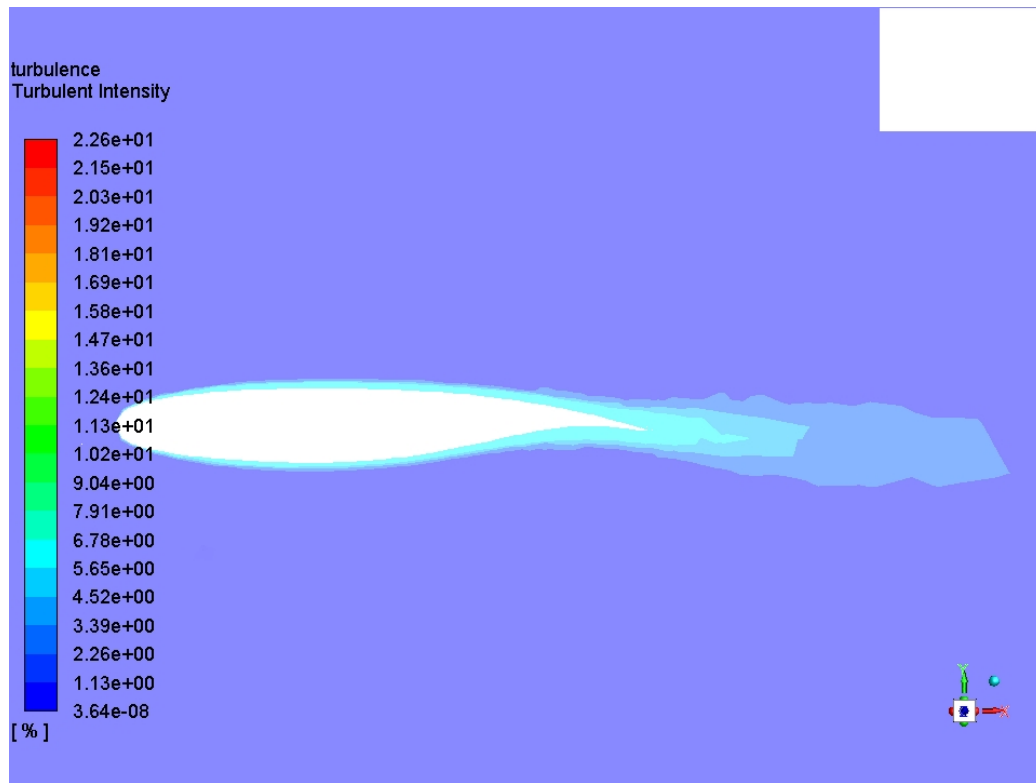
Figure 8.11: Turbulence intensity contour over the airfoil placed before the beginning of the Raked winglet
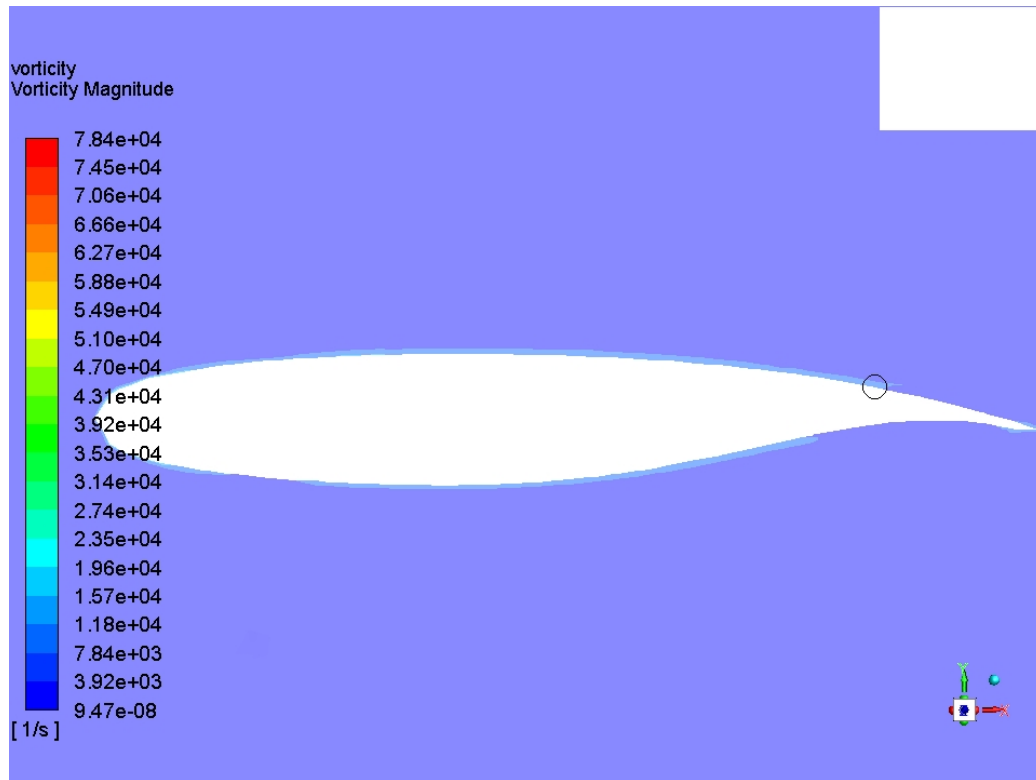
Figure 8.12: Vorticity magnitude contour at the raked wingtip

All these changes on the pressure and turbulence contours are the justification for the increase of lift generation and decrease of drag that we already saw on the previous subsection numerical results.

8.2.3   Blended winglet geometry

The third configuration, the Blended Winglet, is a bit more complex to analyze than the previous ones. This is because the surface of our wing is both on the horizontal and on the vertical plane.
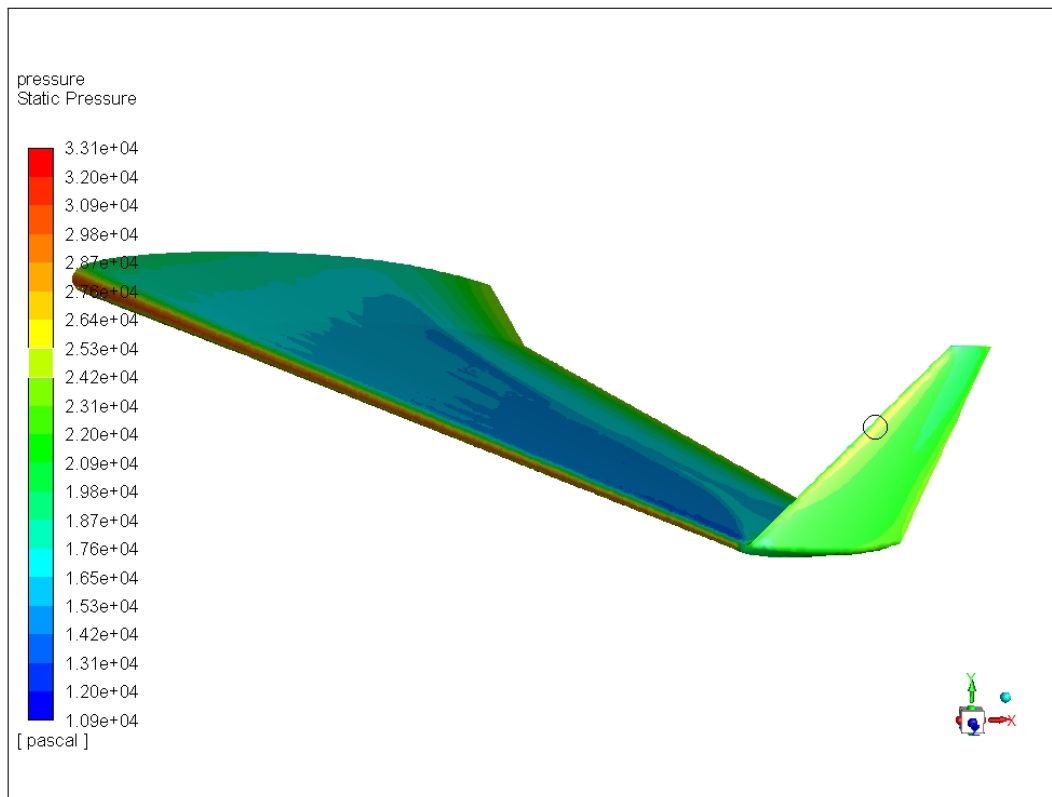
Figure 8.13: Static Pressure 3D-View over the wing surface: Blended configuration

In Figure 8.13. we can already see some differences with respect to the previous cases. For this configuration, the pressure increase on the leading edge seems to be less spread over the wingspan than in the Raked case, but the dark blue is widely spread along the chord up to nearly half of it. If we focus our attention on the extrados, near the winglet's root, we can see that there is another blue zone in the whereabouts of the intrados' curvature

increase. These preliminary observations seem to support the numerical results we obtained in subsection 8.1. where Blended configuration is the one generating more lift than the others.

In addition to this, we can already observe that the static pressure on the outer part of the winglet (the intrados) suffers an increase, up to light green levels, as we can see on the circular marker, which will potentially generate some lift along the z-axis. This will contribute to the lateral stability of the plane and can also contribute to the vertical lift. This lift generated, if the angle of the blended wingtip were bigger, would mean a higher contribution to the overall lift generation as the vertical component of the vector would be larger.

Figure 8.14: Static Pressure distribution over the blended winglet symmetrical airfoil

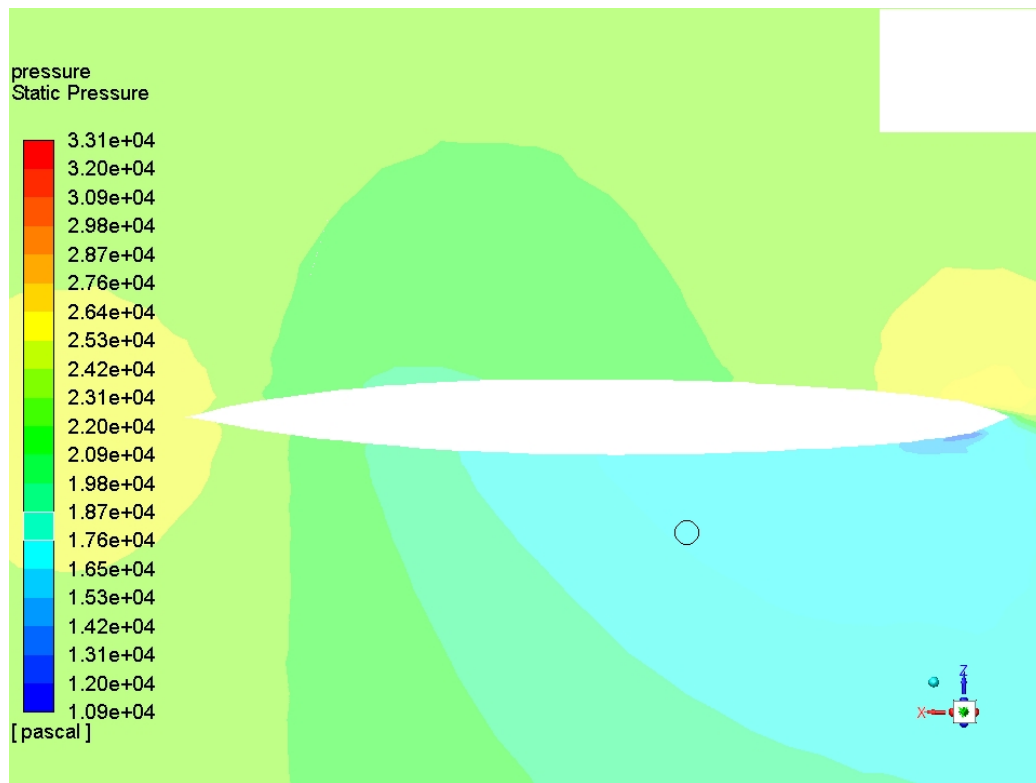By placing an horizontal plane cutting the Blended Winglet at a certain height it will be possible to generate Figure 8.14. In this screenshot, the flow is still flowing in X-axis direction. The system or reference has been turned around in order to properly cut and view the airfoil.

Figure 8.14 allows us to check that there is indeed some generation of an aerodynamic force along the z axis. Although the airfoil used to build the winglet up is symmetrical as explained in previous sections, some changes on the pressure distribution can be spotted. They are generated due to the difference in pressure between the inner and outer surfaces which is related to the flow attempt to go from the intrados to the extrados.

As we can see from the color contours, the aerodynamic force will be generated in the -z direction, which means it will be pointing towards the wing root. This force will be bigger near the leading edge and weaker near the trailing edge, which might provoke a slight bending momentum.

Another important fact with regard to Figure 8.14 is that we can see how the pressure drop on the Trailing Edge is not bounded to the winglet, but it also continues a bit after the end of the section. This means there will also be some turbulence generation in that zone.

Once this particular feature has been analyzed, we can jump into comparing the vertical contours generated by the Blended configuration with the other configurations' already studied. The tool plane has been placed, once more on the equivalent spot to where the winglet's root is located, on the equivalent wingspan position no-winglet configuration.

Figure 8.15 shows how the static pressure is distributed for this case. We can easy see that the configuration differs a lot from the other cases previously exposed.

The pressure drop on the extrados is affected by the winglet vertical walls, and therefore there is a combination of pressure drops, one regarding the wing itself and another one relative to the winglet's extrados. This will mean that the Blended case wingtip lift generation is boosted, in a larger amount than with the Raked winglet's effect. The intrados pressure distribution behaves normally, as the Blended winglet only affects the upper part of the airfoil.
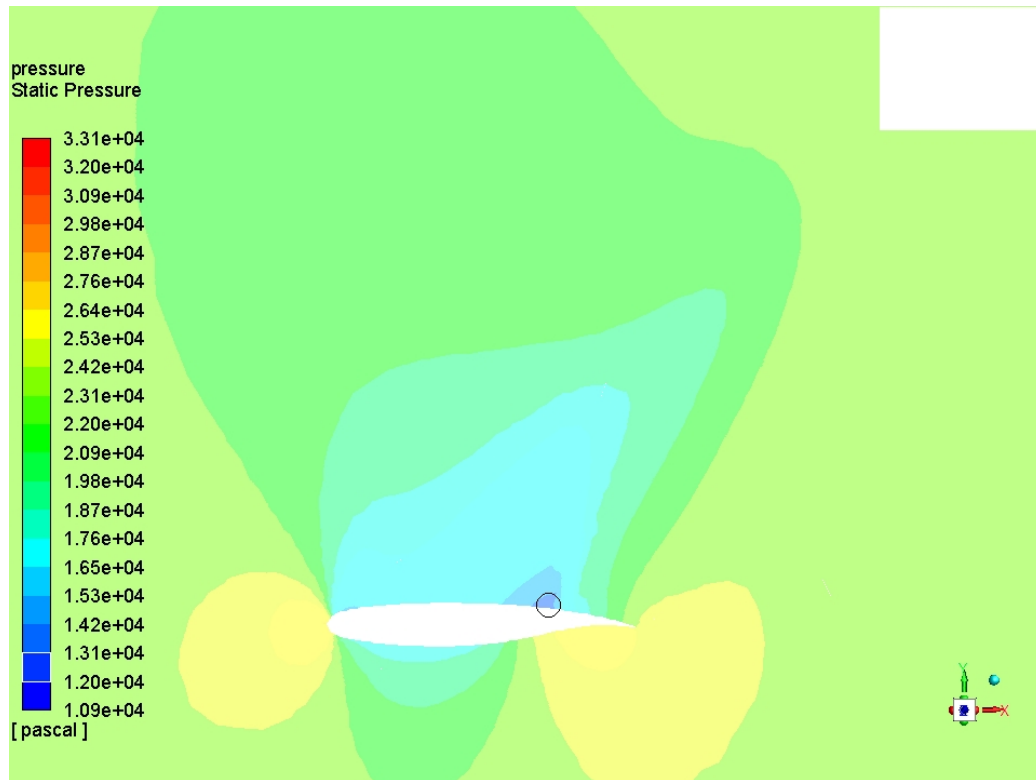
Figure 8.15: Static Pressure distribution over the airfoil placed before the beginning of the Blended winglet

The static pressure decrease near the trailing edge, down to dark blue values, looks like if a weak shock wave would have been generated. This can be said due to how close the isopressure lines are, as they show a fast deceleration of the fluid.

As we did in all the previous cases, we shall analyse in Figure 8.16 the Mach number distribution in order to see if the shock wave characteristics appear.

Indeed, if we check Figure 8.16, it is possible to observe an important increase of the Mach number and a drastic drop from supersonic values down to subsonic values, in the same place as we spotted the pressure drop in

Figure 8.15.on the Mach number on the same spot we just highlighted. This drastic decrease corresponds to the shock wave we intuited before. As we shall see in Figure 8.18, it will have an effect on the drag generated. This is why Blended Case has the larger CD of all the cases, as seen in section 8.1..
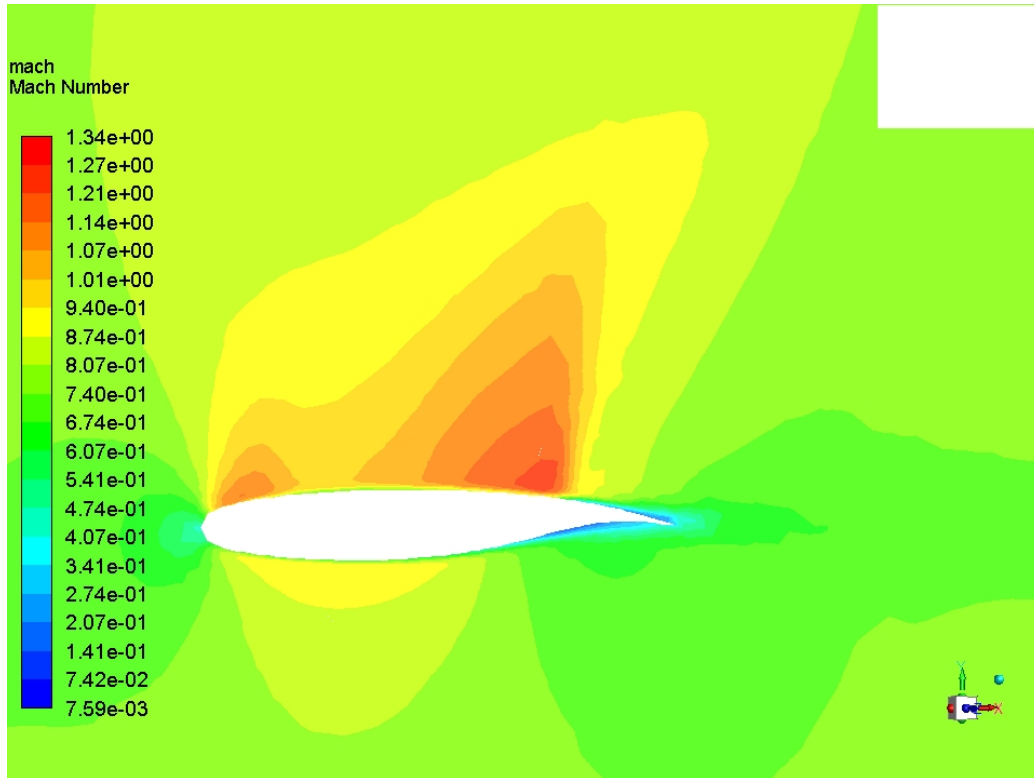
Figure 8.16: Mach number distribution over the airfoil placed before the beginning of the Blended winglet

In Figure 8.17, we can identify the pressure distribution corresponding to the middle wing cutting plane that we already used in Figures 8.3 and 8.9. This extra tool plane brings once more the view of an unperturbed pressure distribution. Once more, we can see that the winglet effect is bounded to the surroundings of the wingtip, locally improving the lift generation avoiding it to drop due to the vortexes influence and reducing the induced drag.
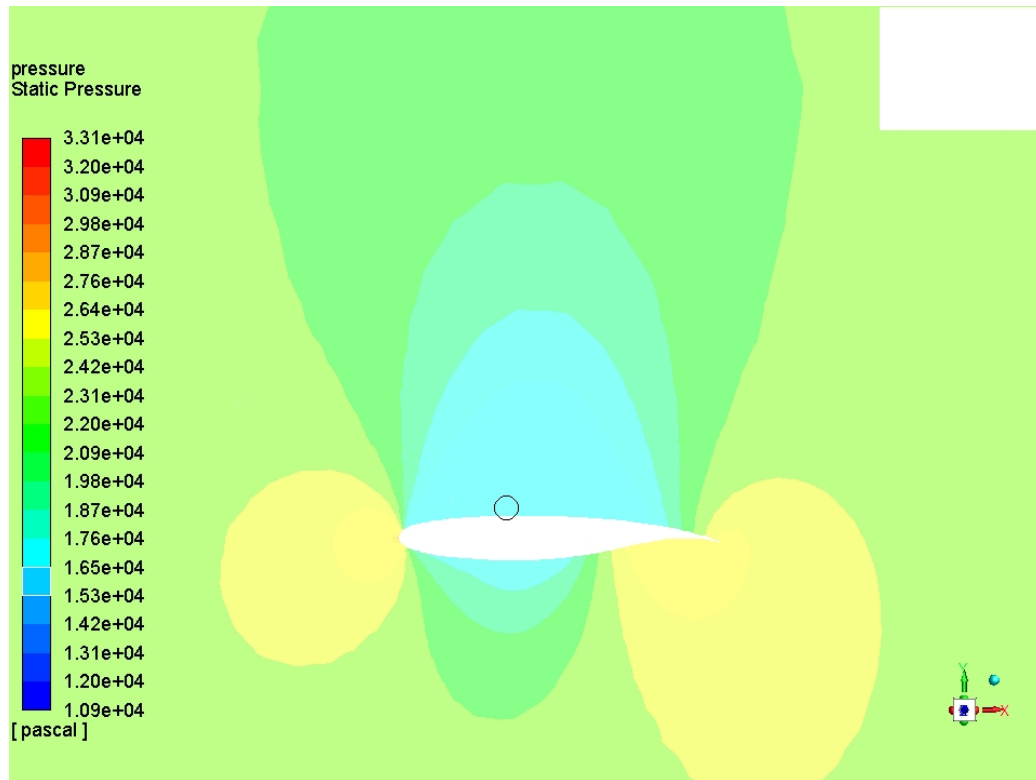
Figure 8.17: Static Pressure distribution in the middle of the wing - Blended Geometry

The following Figures 8.18 and 8.19 show the turbulence intensity distribution. The first of them is generated thanks to a tool plane that cuts the Blended winglet, while 8.19 is supported by a the same vertical plane we have used for the static pressure contours.

In Figure 8.18 we can see the turbulent wake generated by the presence of the winglet. If we focus now our attention on the rear part of the airfoil, we can see that the turbulent intensity values reach the scaled maximum. This value is reached due to the interaction of the flow with the union between the winglet and the wing.

Additionally, we can extract from this contour distribution that the turbulent boundary layer is also present on the winglet's surface.
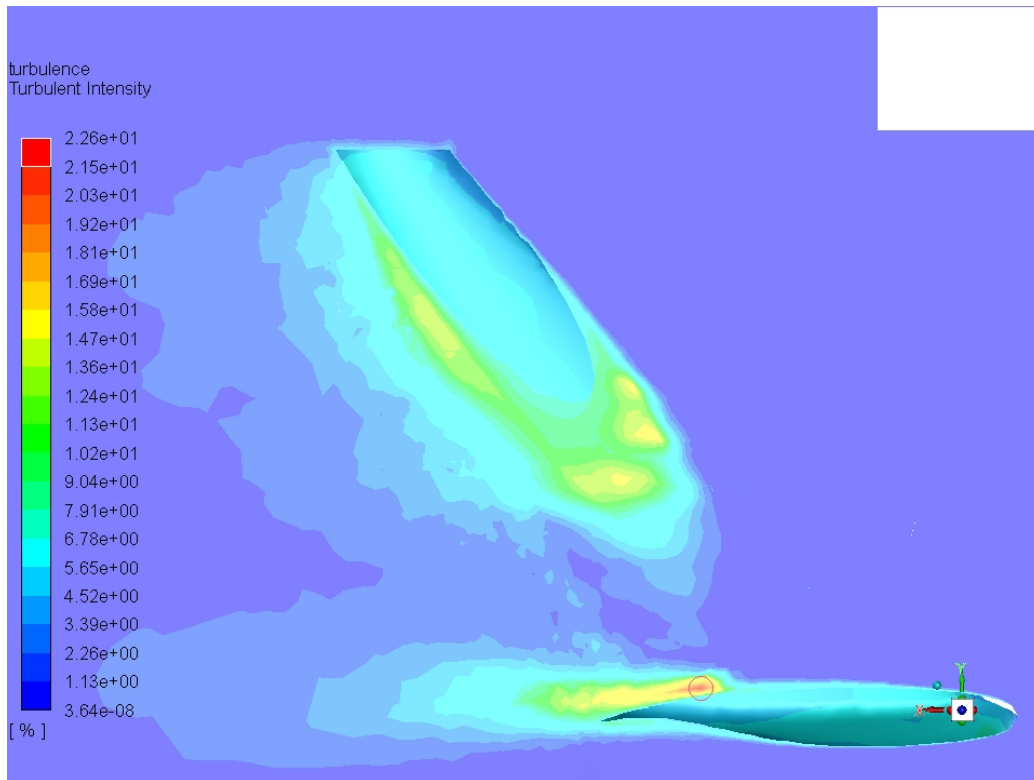
Figure 8.18: Turbulence intensity contour on a plane cutting the blended winglet geometry

In order to compare this configuration to the previous one, we shall also analyze Figure 8.19, as it is the equivalent contour distribution to Figures 8.11 and 8.5 for the Blended case. Thanks to this view, we can see that the boundary layer is much more energized than in the Raked or no-winglet configurations which means it is thinner and therefore generates a smaller wake.
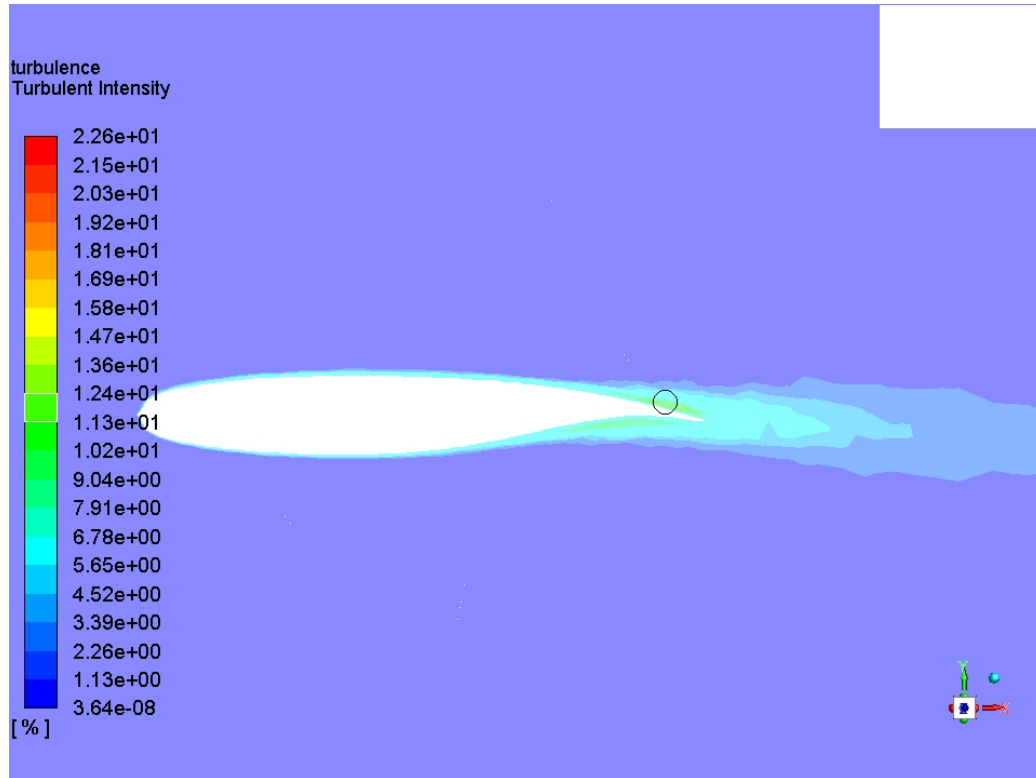
Figure 8.19: Turbulence intensity contour over the airfoil placed before the beginning of the Blended winglet

Finally, Figures 8.20 and 8.21, shall show the vorticity magnitude distribution. It is not as visible as in the no-winglet case, but we can intuit that there is a bigger vorticity generation due to the winglet-wing interference than with the Raked configuration. Nonetheless, both on the airfoil and on the winglet, its values are really low and therefore we can conclude the turbulent layer will not be detached, which seems reasonable.
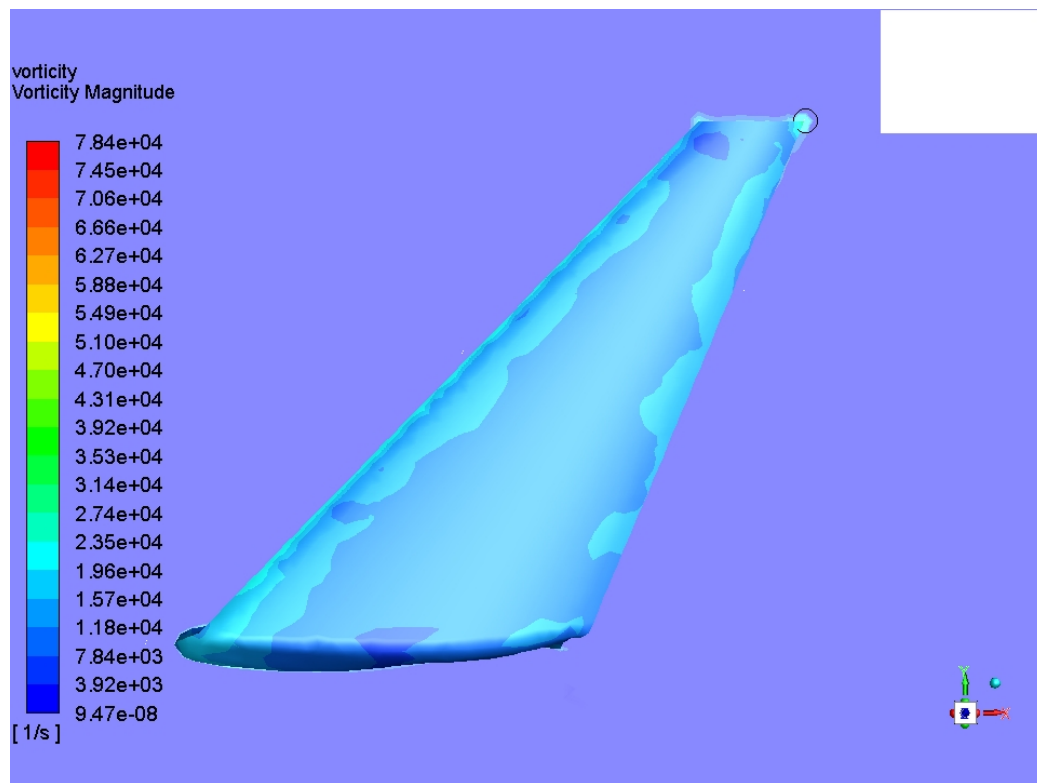
Figure 8.20: Vorticity magnitude contour on a plane cutting the Blended Winglet
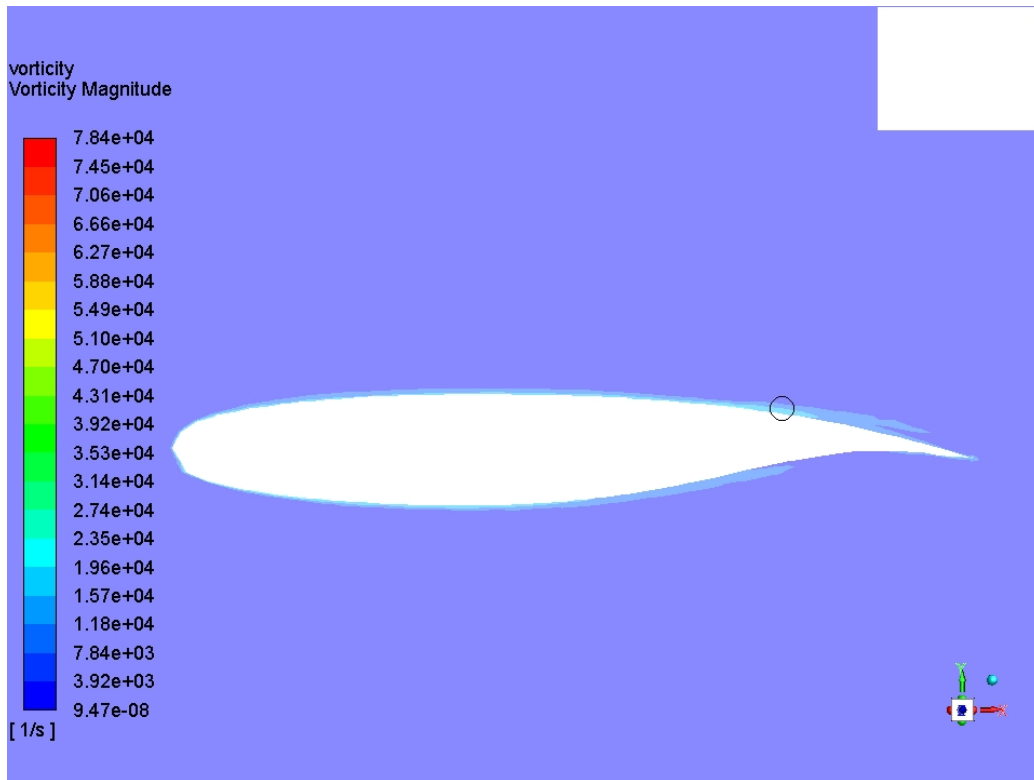
Figure 8.21: Vorticity magnitude contour next to the Blended wingtip

8.2.4   Endplate winglet geometry

This is the last case that we shall analyze on this project. As we can see in Figure 8.22, the pressure distribution is similar to the one over the Raked geometry's winglet.The pressure drop near the leading edge looks like the one we could see in Figure 8.13 for the Blended case. This time, there is not a strong second drop near the TE.

As we could see in Figure 8.13 for the Blended geometry, the vertical winglet outer part (intrados) is suffering the efforts from relatively high pressures. They are lower than in the Blended case though. We can see that as in the Blended case all the surface was set with light green whereas we can see some blue colors on the endplate winglet surface.
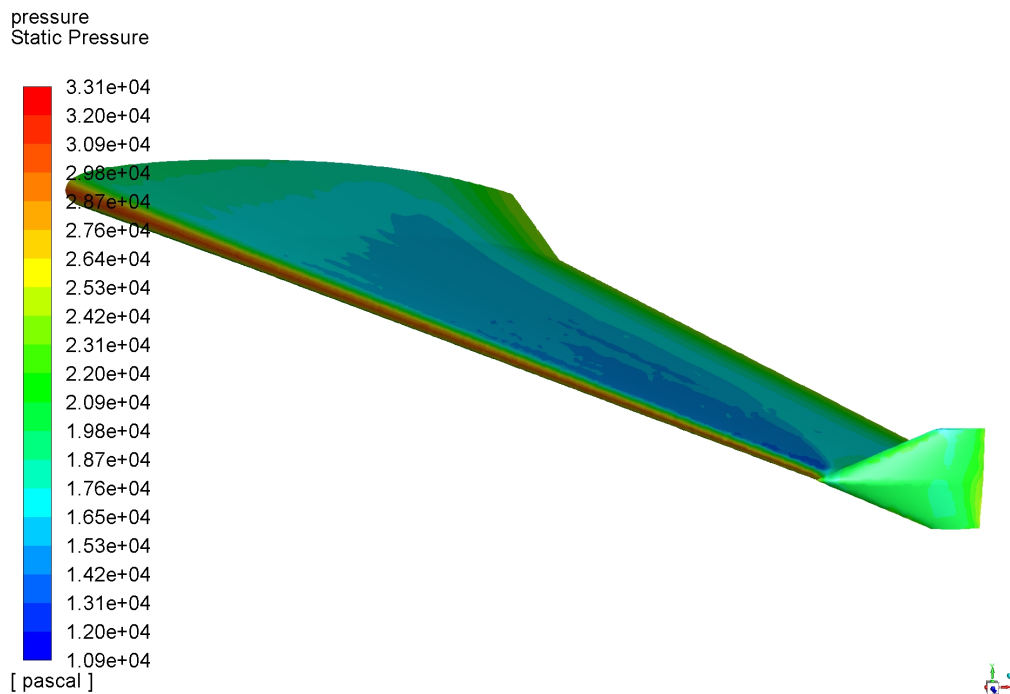
Figure 8.22: Static Pressure 3D-View over the wing surface: Endplate configuration

As we did with the Blended case, two planes have been performed for the pressure distribution analysis. In Figure 8.23, the plane is located in the equivalent place as the one of the no-winglet case would be (its wingtip). For the Figure 8.24, the plane has been performed far from the winglet device.

Then, focusing on Figure 8.23, it is possible to observe a similar effect caused by the winglet on the upper pressure distribution to the one caused by the Blended winglet: the two humps belonging to the extrados pressure distribution are much flatter for the endplate configuration than for the blended case.
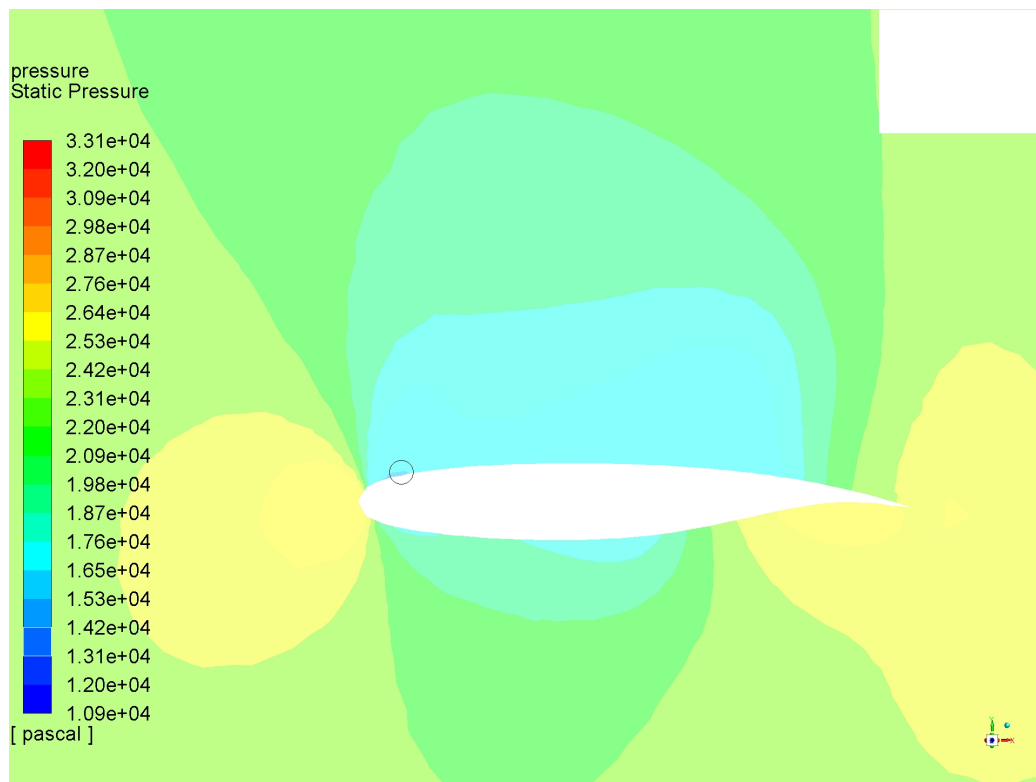
Figure 8.23: Static Pressure distribution over an airfoil section next to the endplate winglet

In the zone of the curvature change near the trailing edge, there are some differences, though. The increase of pressure at the intrados is not as big as

in the blended case, and in fact it seems to be delayed to a closer zone to the TE. That small change on the intrados pressure distribution is related to the fact that the endplate winglet grows vertically both in the positive y direction and in the negative y direction. As we can see, the contours present smaller values which means that as it happened with the Blended winglet, the vertical wall of the Endplate generates a pressure distribution that interacts with the pressure scheme related to the airfoil, reducing in this case the pressure both on the intrados and on the extrados.

This explains why, although the Blended and the Endplate configuration seem to follow the same principle, the resulting effect with regards to the lift generation is much better on the Blended one.

The big difference comes from the drag point of view though. As there is no shock wave generated and there lift generated is lower, the drag this configuration will suffer will be less than the one affecting any of the other configurations.

The absence of shock wave is supported by the view on Figure 8.24. As in the Blended case, we can see two main acceleration zones but they are as intense in the endplate case, and therefore now sudden drop of the Mach number appears, which means, no shock waves have been generated.
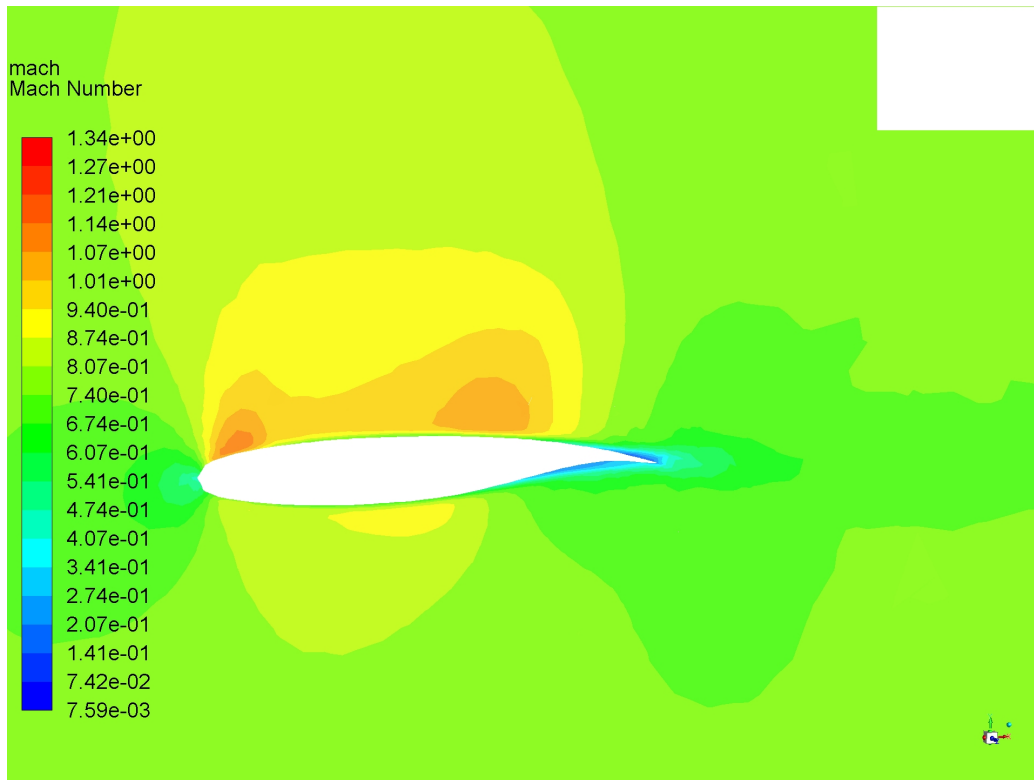
Figure 8.24: Mach number distribution over the airfoil placed before the beginning of the Endplate winglet

As for the pressure distribution in a zone not affected by the winglet, we still are obtaining more or less the same scheme, as we can appreciate in Figure 8.25. All four cases have shown this behavior on an airfoil in the middle of the wingspan.
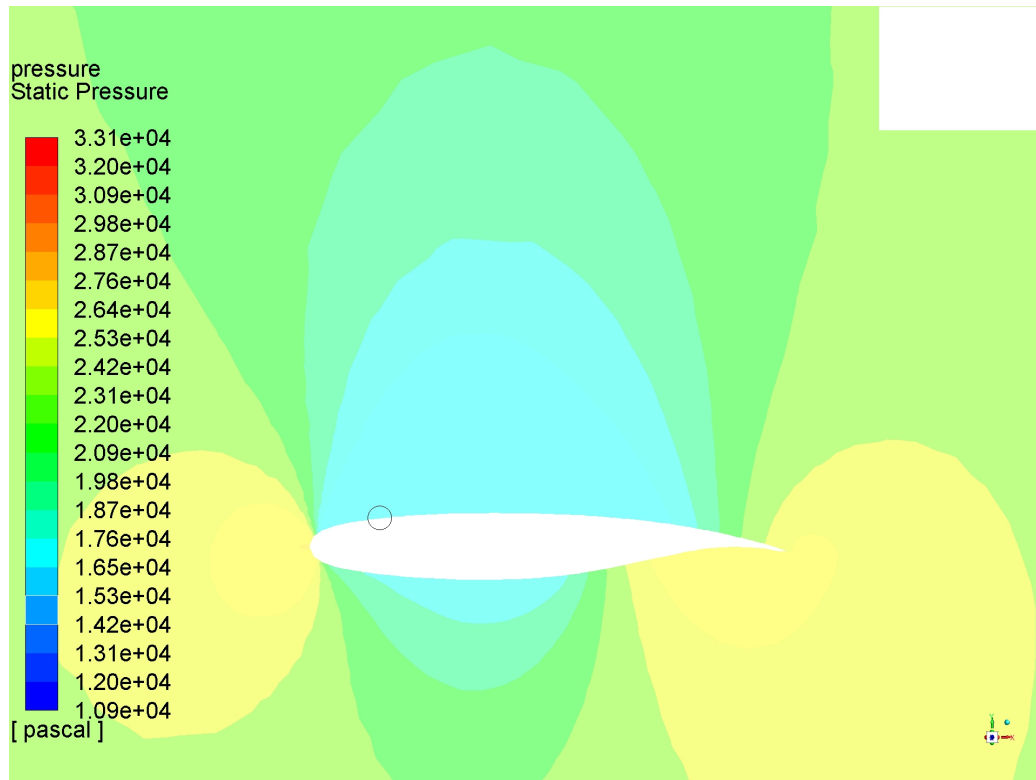
Figure 8.25: Static Pressure distribution in a middle section of the wing - Endplate Geometry

If we now focus on Figures 8.26 and 8.27 which related to the turbulence intensity, we shall distinguish two tool planes. One is placed as in all previous cases near the winglet's root and the other one is cutting it in half.

Figure 8.26. shows the plane which is close to the winglet, in the equivalent position to the one used for the no-wingtip case. Thanks to this view, we can recognize what we already intuited: the turbulence wake generated in the end-plate configuration is the smallest and the weakest one out of all the other configurations. On this Figure the turbulent boundary layer can also be spotted, similarly to the other configurations.
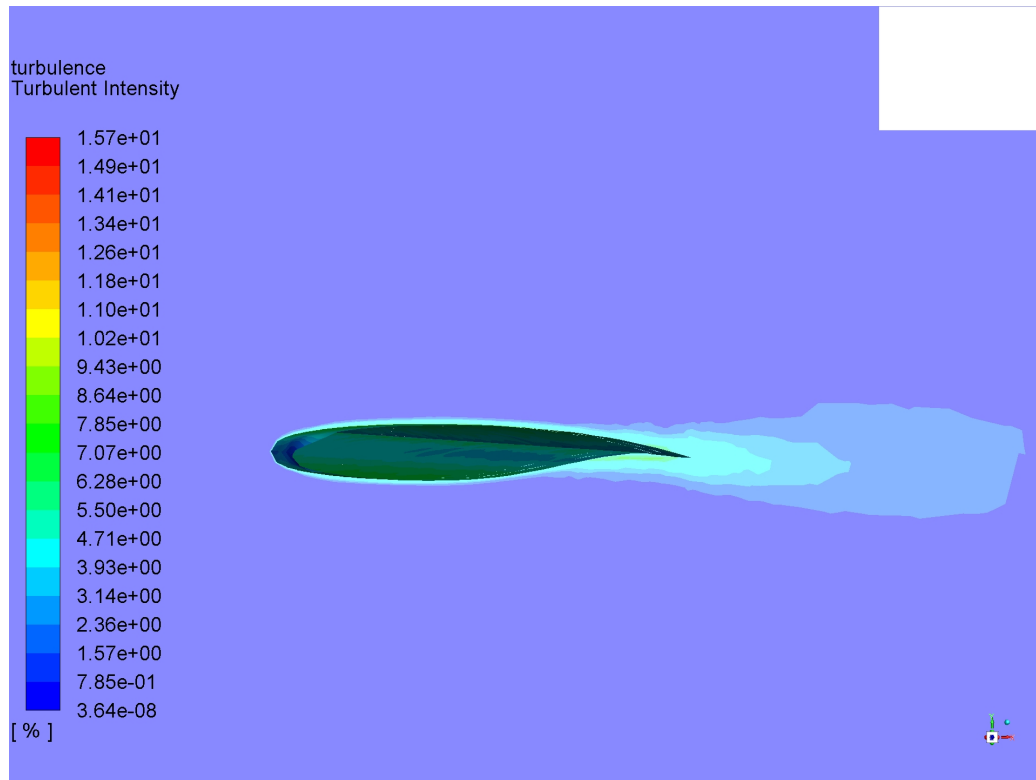
Figure 8.26: Turbulence intensity contour near the wingtip on endplate configuration

In Figure 8.27., the tool plane is cutting the end-plate in half. Thanks to this positioning, it is possible to see the turbulent boundary layer over the winglet and how it evolves. Again, the low values for this turbulent wake are the most important factor we must highlight. Then, it is also interesting to say that there are three separated main wakes, one provoked by the airfoil TE and the other two have their origin on the tips of the winglet. Its effect is symmetric to the horizontal plane as we can also recognize from this Figure 8.27.. This feature shall contribute to the longitudinal stability of the aircraft.
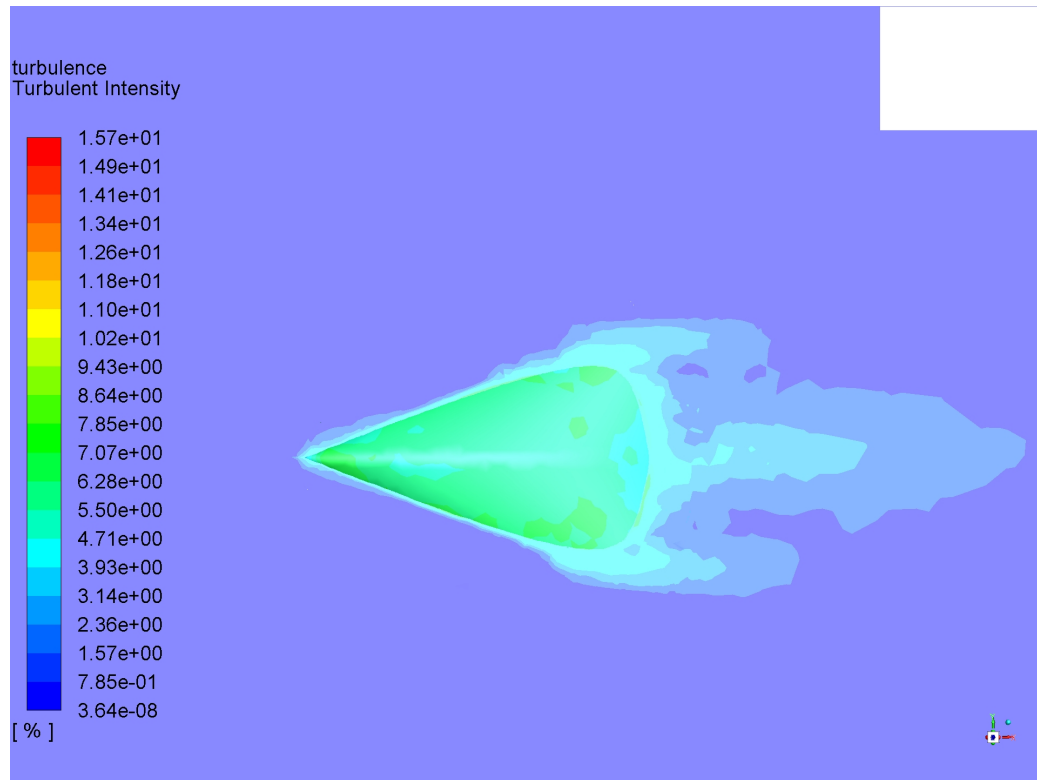
Figure 8.27: Turbulence intensity contour at the endplate wingtip

Once more, we need to check if the boundary layer is detached. To do so, Figure 8.28 is the key tool. It represents the vorticity magnitude distribution along the airfoil section and on the winglet surface.

It is possible to spot on Figure 8.28, that vorticity presents low values, which once more supports the thesis that the boundary layer does not detach from the surface.
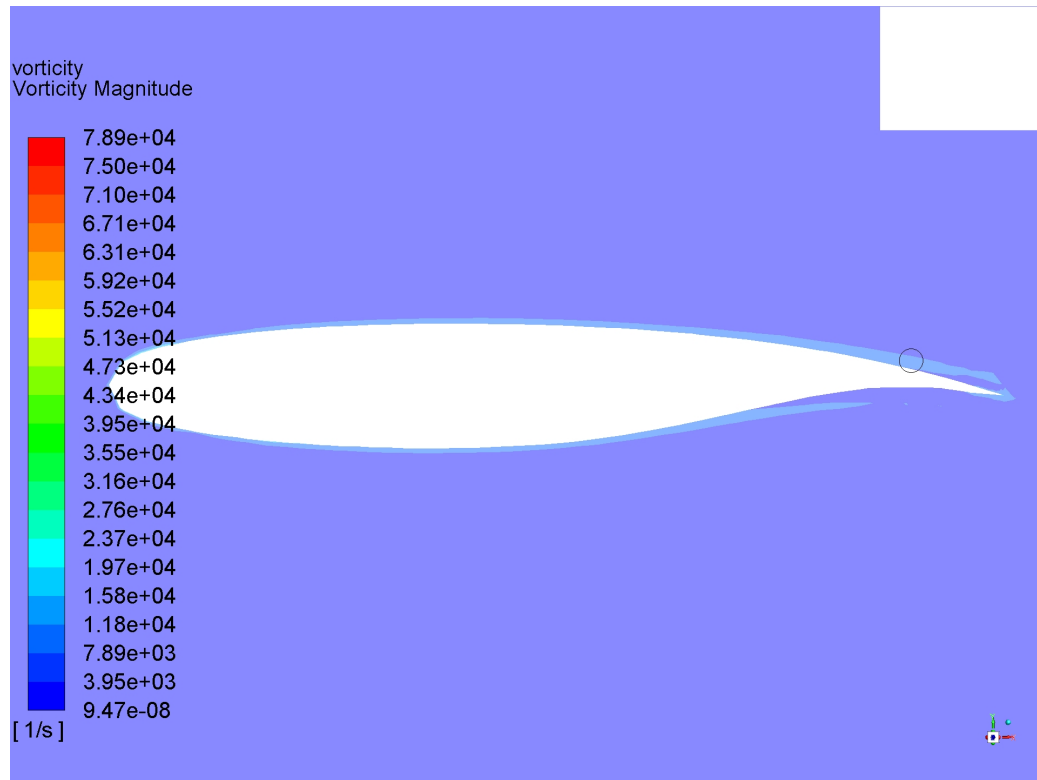
Figure 8.28: Vorticity magnitude contour at the Endplate wingtip

9

Conclusion

After checking all the results obtained from the Computational Fluid Dynamics analysis performed, it is now possible to reach some conclusions with regard to the overall performance of each geometry and to compare this performance to that of the other wingtip devices.

Throughout the previous chapters, the reader has been able to discover all the steps that any research project must follow. In order to review all the results obtained, we should bring up once more the question: why this projects has been performed?

It is our aim to compare four winglet geometries implemented on the same wing in order to clarify which benefits each of them imply and why each aircraft manufacturer uses one configuration or another one.

The first conclusion we can get from this is that there is no straightforward answer for our question. As this study has been performed only for the cruise segment, more data is needed if our aim is to be more precise in distinguishing all the pros and cons for each of the geometries in each of the possible flight conditions. Therefore, we are not able to choose a configuration that performs perfectly in all the flight regimes with the data this

project provides.

Indeed, for any industrial research project, the current document would be the preliminary approach in order to settle the goals.Nonetheless, some interesting conclusions can be extracted from the calculations performed.

As a start up it is an interesting exercise to summarize and combine the numerical data implemented on the **Numerical results** section. As we have both lift and drag net coefficient values for all the configurations, a good measurement can be to plot the aerodynamic efficiency. This key parameter also known as lift/drag ratio will determine any aircraft overall aerodynamic characteristics.

In Figure 9.1 we can observe the four ratios distributed. It is remarkable that the dispersion of the three winglets is low if we do not count the no winglet geometry. This chart shows that as we can intuitively think, if no wintip is applied, the 3D-Flow effect will affect notably the overall performance of the wing and therefore its aerodynamic efficiency will be low.

Once the no-winglet configuration is discarded, we can see that the best aerodynamic performance is the one of the blended winglet, although it presents higher drag coefficient. The high lift performance is the characteristic why this feature is implemented in short cruise-stage aircrafts. It helps in the climb and approach phase as the pilot needs to put less stress on the engine and on the structure to generate more upwards force.

It is followed by the raked winglet geometry. It is a balanced configuration and this is why those planes whose main segment is the cruise use it. In cruise conditions which we are studying now, Raked winglet can reduce the fuel consumption in such a way that the range of the airliners witnesses an important increase.

Endplate configuration is the oldest one regarding the technological and scientific development. Nevertheless, it sets an important difference with regard to the wing with no wingtip device. It is the one with less drag generation and although it will need more effort from the engines in order to get higher speeds (for generating the same amount of lift than the other winglet geometries), this can benefit also the take-off and approach phases, where the

induced drag becomes really important due to the high-lift devices deployment during both stages. This is why many short-cruise phase aircrafts also use it. We can say then, that despite its lower performance with respect to the other configurations, it does affect positively the flow behavior over the wing.

Aerodynamic efficiency ratio
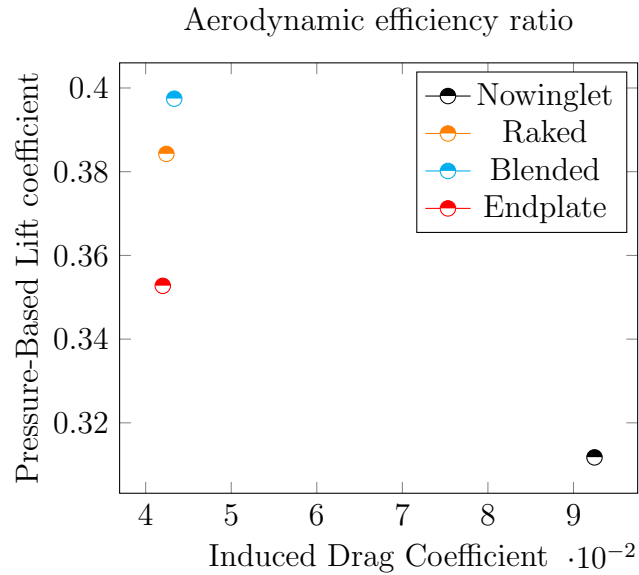
Figure 9.1: Pressure-based Aerodynamic efficiency comparison between geometries

From the graphical results it can be extracted that the main result of the winglets is that they avoid the loss of lift generation on the wingtip, as they avoid the interference of the vortexes with the pressure distribution on the lifting surfaces. In the case of the Blended and Endplate winglets they do so by moving their origin of the turbulent whirlwind far from the wing surface, either only above it as in the Blended case or both above and below the surface plane as in the Endplate case.

As for the Raked winglet, the sweep angle provokes the reduction of the turbulence intensity and therefore, although the added surface generates a small amount of lift, the main feature is that it avoids the downwash affect to the actual lifting surfaces, generating a smaller induced angle of attack.

We can also say that the winglet only affects to the zone near the wingtip, whose lift generation capacity is modified when no winglets are used.

Out of this study we can also see many ways to continue the research and continue extracting conclusions. The most obvious one is related to the flight regimes.

Right now, these devices have only been tested on cruise regime, at 0 angle of attack. It would be interesting to check their performance when the angle of attack increases even up to stall conditions. It can also be illustrative to change the flight Mach number by changing the speed or the altitude (by changing the temperature, density or pressure characteristics).

Another important factor would be to test their contribution towards the lateral stability of the aircraft to see if they affect this factor ad if they do in a positive or negative way.

Then, all these variations could be also implemented for other flight phases, such as take-off or landing, in order to finally decide if Blended and Endplate- wingtips are actually better in those conditions.

More improvements can be also related to the development and quality of the measuring features. The development of a much more accurate mesh can show more details on the turbulent boundary layer.

And finally, to perform actual measurements on the wind tunnel in order to validate the software results and to gather more empirical data with regard to the torsion moments at the wing root, depending of the wing tip.

All in all, this project aim has been accomplished as it provides some good material for the Aerodynamics Lab practice and it shows some preliminary conclusions with regard to the performance of the wingtip devices that are consistent with the experience and the real strategies that aircraft manufacturers implement on their models.

Bibliography

[1]   aviation admin. *Sharklets, Raked Wing tips, Split Scimitar Winglets and Advance Technology Winglets.* URL: `http://aviationthrust.in/notes/sharklets-raked-wing-tips-split-scimitar-winglets-advance-technology-winglets/`.

[2]   Inc. ANSYS. *ANSYS Help Viewer.* Canonsburg, USA: ANSYS, Inc., 2017.

[3]   SHARCNET project - Canada. *Inflation Option.* 2016. URL: `https://www.sharcnet.ca/Software/Ansys/16.2.3/en-us/help/wb_msh/msh_Inflation_Opt_Global.html`.

[4]   Leap australia CFD Blog. *Meshing.* Jan 6, 2012. URL: `https://www.computationalfluiddynamics.com.au/tips-tricks-inflation-layer-meshing-in-ansys/`.

[5]   cfd-online. *Meshing.* 2012. URL: `https://www.cfd-online.com/Wiki/Meshing`.

[6]   cfd-online. *turbulent viscosity limited to viscosity ratio of 1.000000e+05 in 511831 cells.* 2011. URL: `https://www.cfd-online.com/Forums/fluent/92302-turbulent-viscosity-limited-viscosity-ratio-1-000000e-05-511831-cells.html`.

[7]   Fleugzeuginfo.net. *Airbus A320 Airliner.* 2001-2017. URL: `http://www.flugzeuginfo.net/acdata_php/acdata_a320_en.php`.

[8]   Walter Frei. *Which Turbulence Model Should I Choose for My CFD Application?* 2016. URL: `https://www.comsol.com/blogs/which-turbulence-model-should-choose-cfd-application/`.

[9]   Site developed by Greteman Group. *Official Site Aviation Partners Inc.* URL: `http://www.aviationpartners.com/`.

[10] Charles D. Harris. "The supercritical airfoil: TF-2004-13 DFRC". In: *NASA: Langley Research Center* (). DOI: https://www.nasa.gov/pdf/89232main_TF-2004-13-DFRC.pdf.

[11] 3D HUBS. *What is 3D Printing*. URL: https://www.3dhubs.com/what-is-3d-printing#basics/.

[12] Jr. John D. Anderson. *FUNDAMENTALS OF AERODYNAMICS - Third edition*. New York, USA: McGraw-Hill, Inc., 2001.

[13] Ahmed Al Makky. *CFL Condition*. 2013. URL: http://cfd2012.com/cfl-condition.html.

[14] Xandra Margot. *Lecture notes on Incompressible flow over finite three-dimensional wings*. València, España: Departamento Máquinas y Motores Térmicos, Universitat Politècnica de València, 2015.

[15] Mark D. Maughmer. "THE DESIGN OF WINGLETS FOR LOW-SPEED AIRCRAFT". In: *University Park, Pennsylvania 16802* (). DOI: http://www.mandhsoaring.com/why%20winglets/wl-it.pdf.

[16] Malcom Muir. "WINGLETS... THE ULTIMATE AVGEEK GUIDE". In: *Airline Reporter* (). DOI: http://www.airlinereporter.com/2014/03/winglets-the-ultimate-guide/.

[17] NASA. "NASA Supercritical airfoils: A Matrix of Family-Related Airfoils". In: *technology facts* (). DOI: https://www.nasa.gov/pdf/89232main_TF-2004-13-DFRC.pdf.

[18] Saravanan Rajendran. *Design of Parametric Winglets and Wing tip devices – A Conceptual Design Approach*. Linköping, Sweden: Linköpings Universitet, 2012. URL: https://pdfs.semanticscholar.org/1d88/3f3d95ab38e99ea37fdbc3d37c93c55a9fd3.pdf.

[19] Acquilla S. Hill; Renaldo V. Jenkins and Edward J. Ray. *Aerodynamic Performance and Pressure Distributions for a NASA SC(2)-0714 Airfoil Tested in the Langley 0.3-Meter Transonic Cryogenic Tunnel*. València, España: NASA TM-4044, 1988.

[20] Jose Pedro Magraner Rullan. *11889 Mecánica de vuelo I - Tema 00 Procedimiento 01 Describe el modelo de atmósfera I.S.A y el sistema de unidades S.I.* Valencia, Spain: Departamento Máquinas y Motores Térmicos, Universitat Politècnica de València, 2016.

[21]   Jose Pedro Magraner Rullan. *11889 Mecánica de vuelo I - Tema 00 Procedimiento 02 Aerodinámica*. Valencia, Spain: Departamento Máquinas y Motores Térmicos, Universitat Politècnica de València, 2016.

[22]   Technical Data Support and Services. *AIRPLANE CHARACTERISTICS FOR AIRPORT PLANNING*. 31707 Blagnac Cedex, FRANCE: AIRBUS S.A.S, 2011.

[23]   Sysmcape. *Reynolds-Averaged Navier-Stokes Equations*. 2009. URL: `http://www.symscape.com/reynolds-averaged-navier-stokes-equations`.

[24]   Advanced Transport Technology Office THEODORE G. AYERS. "SUPERCRITICAL AERODYNAMICS WORTHWHILE OVER A RANGE OF SPEEDS". In: *Astronautics and Aeronautics: a publication of the American Institute of aeronautics and astronautics* (). DOI: `https://www.nasa.gov/pdf/89232main_TF-2004-13-DFRC.pdf`.

[25]   Waldo1. "WILLIAM E. SOMERVILLE OF COAL CITY ILLINOIS 1870-1950". In: *ILLINOIS AVIATION HALL OF FAME NEWSLETTER* (). DOI: `http://www.ilavhalloffame.org/Newsletters/5Newsletter.pdf`.

[26]   Commercial Aviation Services; William Freitag Winglet Program Manager and Aerodynamics E. Terry Schulze Manager. *Blended winglets improve performance*. 2009. URL: `http://www.boeing.com/commercial/aeromagazine/articles/qtr_03_09/article_03_1.html`.

A

Budget

In this section all the costs that this project have implied will be presented. Thanks to these figures it is possible to balance the expense that this kind of basic study implies for an aerospace corporation.

Two main groups of resources invested on this project can be highlighted. On the one hand, the human resources which include:

- 1 Senior Lecturer;
- 1 Manufacturing Technician;
- 1 Research Assistant in CFD;
- 1 Aerospace Engineering Student.

On the other hand, the material resources invested on this projects are listed below:

- Software licenses;
- IT System;
- Manufacturing tools;
- Perishable equipment.

A.1   Fractional Expenses Budget

Throughout this project, all the procedures that have been followed imply a cost as they have consumed some of the resources previously listed. In this section these partial costs shall be reported.

Definition	Measurement [h]	Unitary Cost [€/h]	Total Cost [€]
Aerospace Engineering Student*	50 (2 ECTS)	3.26	163
Software License	50	1	50
SubTotal:			**213**

Table A.1: Fractional expenses budget related to information collection and to CAD models development

Definition	Measurement [h]	Unitary Cost [€/h]	Total Cost [€]
Aerospace Engineering Student*	60 (2.4 ECTS)	3.26	195.6
Research Assistant in CFD	2	11	22
Software License	50	1	50
SubTotal:			**267.6**

Table A.2: Fractional expenses budget related to meshing process

Definition	Measurement [h]	Unitary Cost [€/h]	Total Cost [€]
Aerospace Engineering Student*	100 (4 ECTS)	3.26	326
Senior lecturer	15	30	450
Software License	360	1	360
SubTotal:			**1136**

Table A.3: Fractional expenses budget related to Set Up of the cases and calculations

Definition	Measurement [h]	Unitary Cost [€/h]	Total Cost [€]
Aerospace Engineering Student*	65 (2.6 ECTS)	3.26	221.9
Manufacturing Technician	15	11	165
SubTotal:			**386.9**

Table A.4: Fractional expenses budget related to Manufacturing process.

Definition	Measurement [h]	Unitary Cost [€/h]	Total Cost [€]
Aerospace Engineering Student*	25 (1 ECTS)	3.26	81.5
Senior lecturer	5	30	150
Software License	10	1	10
SubTotal:			**241.5**

Table A.5: Fractional expenses budget related to the postprocessing and work the report out.

*12 ECTS are assigned for this project. Each ECTS is equal to 25 working hours. The total cost for the UPV of these 12 ECTS equals 978,12 €.

Definition	Measurement [Units]	Unitary Cost [€/Unit]	Total Cost [€]
Laptop (20%)	1	160	160
Stationery shop materials	3	30	90
3D Printing machine (10%)	2	180	360
3D Printing material (Hibs Zortrax 800g pure black)	544 (gram)	0.04875	26.52
Dremel (10%)	1	10	10
Other manufacturing materials	20	0.5	10
SubTotal:			**656.52**

Table A.6: Fractional expenses budget related to perishable equipment

A.2   Total expenses Budget

In the next table all the previous SubTotals are merged in order to know the total amount of money invested on the project.

Definition	Measurement [Units]	Unitary Cost [€/Unit]	Total Cost [€]
Information collection and CAD development	1	213	213
Meshing process	1	267.6	267.6
Set Up and calculations	1	1136	1136
Manufacturing process	1	386.9	386.9
Postprocessing and report development	1	241.5	241.5
Perishable equipment	1	656.52	656.52
Total:			**2901.52**

Table A.7: Fractional expenses budget related to perishable equipment